JOURNAL OF THE AERONAUTICAL SCIENCES

VOLUME 9 NOVEMBER, 1942 NUMBER 13

Ground Vibration Tests

C. D. PENGELLEY*

Curtiss-Wright Corporation

ABSTRACTS

The dynamics of a rigid body having two degrees of freedom is presented. The complete solutions for nodal points and coupled frequencies are obtained. The general solution for the nodal positions is presented in graphic form, which provides not only a physical picture of any system but also a rapid means of evaluating the position of the nodes. Charts have been prepared from which the uncoupled frequencies, as required in flutter analysis, may be rapidly evaluated from data observed during vibration tests. Neglect of this item may produce an unconservative error of 20 per cent in the calculated flutter speed.

A theoretic analysis is made of the factors affecting the power and unbalance required to conduct vibration tests. It is shown that for a given amplitude the power absorbed by a wing is roughly independent of airplane size; however, for any given airplane it is from two to sixteen times greater at torsional than bending resonance. At torsional resonance, with one-tenth-in. total motion of the trailing edge, a conventional wing absorbs about 0.0134 hp. Thus, the theoretic power required is negligible, and the choice of a suitable motor depends upon the friction horsepower absorbed by the test equipment.

Numerical examples are presented to illustrate the use of all principal equations and charts.

A discussion is given of the new Curtiss-Wright Universal Vibrator, outlining its major points of interest.

INTRODUCTION

THE PRINCIPAL PURPOSE of this paper is to present some of the methods that have been developed by the St. Louis Plant of the Curtiss-Wright Corporation during vibration and flutter analyses made in the past two years. The fundamental theory covering the motion of a body with two coupled degrees of freedom has been derived by several writers.[1, 2, 3, 5, 6] However, with regard to coupled frequencies and nodal points, experience has shown that the results obtained in these references are in a form that cannot easily be applied to practical engineering problems. The dynamics of a rigid body (Fig. 1) with two degrees of freedom has been derived herewith in a form which, it is believed, lends itself most readily to the solution of certain vibration problems that often confront the practicing engineer. It has been assumed throughout that the conventional flutter parameters—namely, elastic axis and c.g. location—as well as radius of gyration, have been calculated and, in addition, that the coupled frequencies have been determined experimentally.

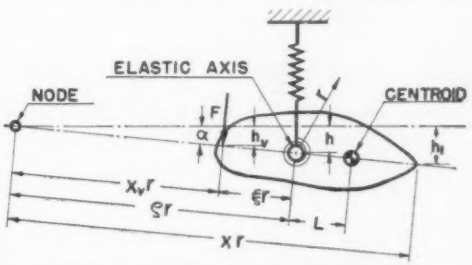

FIG. 1. System with two degrees of freedom. NOTE: X and X_v are scalar quantities and are always considered positive. All other dimensions are shown in positive sense with respect to the elastic axis.

The analyses that follow apply rigorously to a rigid body supported on springs and having two degrees of freedom. As discussed later, it has been assumed throughout that the results obtained from such a system can be applied to actual three-dimensional structures in which the elasticity is distributed throughout the structure itself. Experience, supported by Theodorsen[4] and several other investigators,[5, 6] has justified this assumption. In many cases of airplane vibrations the results can be applied quantitatively with a high degree of accuracy, and in almost every case they can be applied qualitatively.

Solutions to equations have been presented graphically to facilitate practical engineering work, and numerical examples have been worked out to illustrate the applications of the principal charts and equations.

Presented at the Structures Session, Tenth Annual Meeting, I.Ae.S., New York, January 28, 1942.

* Aerodynamicist.

JOURNAL OF THE AERONAUTICAL SCIENCES

VOLUME 9 NOVEMBER, 1942 NUMBER 13

Ground Vibration Tests

C. D. PENGELLEY*

Curtiss-Wright Corporation

ABSTRACTS

The dynamics of a rigid body having two degrees of freedom is presented. The complete solutions for nodal points and coupled frequencies are obtained. The general solution for the nodal positions is presented in graphic form, which provides not only a physical picture of any system but also a rapid means of evaluating the position of the nodes. Charts have been prepared from which the uncoupled frequencies, as required in flutter analysis, may be rapidly evaluated from data observed during vibration tests. Neglect of this item may produce an unconservative error of 20 per cent in the calculated flutter speed.

A theoretic analysis is made of the factors affecting the power and unbalance required to conduct vibration tests. It is shown that for a given amplitude the power absorbed by a wing is roughly independent of airplane size; however, for any given airplane it is from two to sixteen times greater at torsional than bending resonance. At torsional resonance, with one-tenth-in. total motion of the trailing edge, a conventional wing absorbs about 0.0134 hp. Thus, the theoretic power required is negligible, and the choice of a suitable motor depends upon the friction horsepower absorbed by the test equipment.

Numerical examples are presented to illustrate the use of all principal equations and charts.

A discussion is given of the new Curtiss-Wright Universal Vibrator, outlining its major points of interest.

INTRODUCTION

THE PRINCIPAL PURPOSE of this paper is to present some of the methods that have been developed by the St. Louis Plant of the Curtiss-Wright Corporation during vibration and flutter analyses made in the past two years. The fundamental theory covering the motion of a body with two coupled degrees of freedom has been derived by several writers.[1, 2, 3, 5, 6] However, with regard to coupled frequencies and nodal points, experience has shown that the results obtained in these references are in a form that cannot easily be applied to practical engineering problems. The dynamics of a rigid body (Fig. 1) with two degrees of freedom has been derived herewith in a form which, it is believed, lends itself most readily to the solution of certain vibration problems that often confront the practicing engineer. It has been assumed throughout that the conventional flutter parameters—namely, elastic axis and c.g. location—as well as radius of gyration, have been calculated and, in addition, that the coupled frequencies have been determined experimentally.

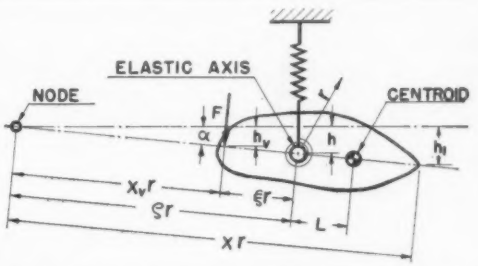

FIG. 1. System with two degrees of freedom. NOTE: X and X_v are scalar quantities and are always considered positive. All other dimensions are shown in positive sense with respect to the elastic axis.

The analyses that follow apply rigorously to a rigid body supported on springs and having two degrees of freedom. As discussed later, it has been assumed throughout that the results obtained from such a system can be applied to actual three-dimensional structures in which the elasticity is distributed throughout the structure itself. Experience, supported by Theodorsen[4] and several other investigators,[5, 6] has justified this assumption. In many cases of airplane vibrations the results can be applied quantitatively with a high degree of accuracy, and in almost every case they can be applied qualitatively.

Solutions to equations have been presented graphically to facilitate practical engineering work, and numerical examples have been worked out to illustrate the applications of the principal charts and equations.

Presented at the Structures Session, Tenth Annual Meeting, I.Ae.S., New York, January 28, 1942.

* Aerodynamicist.

Symbols

(All symbols are in fundamental ft.lb. sec. units)

$*a$	= elastic axis parameter
$*b$	= half chord of wing
B	= wing span
$*C_h$	= bending stiffness coefficient per unit span of two-dimensional wing
$*C_\alpha$	= torsional stiffness coefficient per unit span of two-dimensional wing
F	= force applied by vibrator
g	= acceleration of gravity
$*g_\alpha$, g_h	= damping coefficients
h	= deflection of elastic axis
h_v	= deflection of point of application of F
h_1	= deflection of any reference point
$L = *bx_\alpha$	= distance between c.g. and elastic axis
L_v	= distance between rotors of a twin rotor vibrator
P	= power
$r = *br_\alpha$	= radius of gyration about elastic axis
W	= weight of equivalent two-dimensional body
$W_v r_v$	= unbalance of vibrator
Xr	= distance from node to reference point (always positive)
$X_v r$	= distance from node to vibrator (always positive)
α	= angular deflection (rad.)
ϕ	= phase angle (rad.)
μ, μ_α, μ_h	= see definition following Eq. (19)
$*\kappa$	= mass ratio
$*\omega$	= frequency of applied force (rad. per sec.)
Ω	= frequency of applied force at resonance (rad. per sec.)
ω_2, ω_1	= greater and smaller uncoupled frequencies of system with two degrees of freedom (rad. per sec.)
$*\omega_\alpha$	= uncoupled torsional frequency about elastic axis (rad. per sec.)
$*\omega_h$	= uncoupled bending frequency (rad. per sec.)
Ω_2, Ω_1	= greater and smaller coupled frequencies of system with two degrees of freedom (rad. per sec.)
λ	= $\left(\frac{\text{unbalance of smaller rotor}}{\text{unbalance of larger rotor}}\right)$ for a twin rotor vibrator (positive when rotors are in phase; negative when 180 deg. out of phase)
δL_v	= distance from point midway between rotors to single equivalent rotor of a twin-rotor vibrator
ξr	= distance from elastic axis to applied force (positive when elastic axis lies between c.g. and force)
ζr	= distance from elastic axis to node (positive when elastic axis lies between c.g. and node)
ζ_1, ζ_2	= positive and negative solutions, respectively, for ζ at resonance

Subscript 0 indicates amplitude of oscillating function.

* These symbols are the same as those used by Theodorsen

Theory

Reference is made to the system illustrated in Fig. 1 which represents a rigid body having two degrees of freedom. It is supported at the elastic axis by means of a spring of stiffness C_h, while restraint about the elastic axis is supplied by a coil spring of torsional stiffness C_α. An oscillating force, $F = F_0 \cos \omega t$, is applied at a distance ξr from the elastic axis. The equations of motion may be determined by equating to zero the sum of all forces and moments. Whence

$$\Sigma F = 0$$

$$-(d^2h/dt^2 + Ld^2\alpha/dt^2)(W/g) - hC_h + F = 0 \quad (1)$$

$$\Sigma M = 0 \quad \text{(about elastic axis)}$$

$$-(Ld^2h/dt^2 + r^2d^2\alpha/dt^2)(W/g) - \alpha C_\alpha - F\xi r = 0 \quad (2)$$

Assuming sinusoidal motion and making the following substitutions

$$h = h_0 e^{i\omega t} \qquad \alpha = \alpha_0 e^{i\omega t}$$

$$d^2h/dt^2 = -\omega^2 h_0 e^{i\omega t} \qquad d^2\alpha/dt^2 = -\omega^2 \alpha_0 e^{i\omega t}$$

$$F = F_0 e^{i\omega t}$$

$$C_h/(W/g) = \omega_h^2 \qquad C_\alpha/r^2(W/g) = \omega_\alpha^2$$

Eqs. (1) and (2) become

$$h_0(\omega^2 - \omega_h^2) + r\alpha_0\omega^2 L/r + F_0/(W/g) = 0 \quad (3)$$

$$h_0\omega^2 L/r + r\alpha_0(\omega^2 - \omega_\alpha^2) - F_0\xi/(W/g) = 0 \quad (4)$$

It should be noted that Eqs. (3) and (4) define completely the steady state motion of the body in response to a sinusoidal force of amplitude F_0 and having any frequency ω.

With reference to Fig. 1 it can be seen that the point about which the resultant response occurs at any frequency ω is given by

$$\zeta = h_0/r\alpha_0$$

At resonance, the nodal points and frequencies are given by the particular solution of Eqs. (3) and (4) (i.e., for $F_0 = 0$).

Therefore, when ω is equal to the resonant frequency Ω and ζ is substituted for $h_0/r\alpha_0$, Eqs. (3) and (4) become

$$\zeta(\Omega^2 - \omega_h^2) + \Omega^2 L/r = 0 \quad (5)$$

$$\zeta\Omega^2 L/r + (\Omega^2 - \omega_\alpha^2) = 0 \quad (6)$$

whence

$$\zeta = \frac{[(\omega_\alpha/\omega_h)^2 - 1] \pm \sqrt{[(\omega_\alpha/\omega_h)^2 - 1]^2 + 4(\omega_\alpha/\omega_h)^2(L/r)^2}}{2L/r} \quad (7)$$

$$\Omega^2 = \frac{(\omega_\alpha^2 + \omega_h^2) \pm \sqrt{(\omega_\alpha^2 + \omega_h^2)^2 - 4\omega_\alpha^2\omega_h^2(1 - L^2/r^2)}}{2(1 - L^2/r^2)} \quad (8)$$

By inspection of Eq. (7) it can be seen that the sign before the radical always determines the sign of ζ, the positive value being defined as ζ_1 and the negative by ζ_2. Therefore there are always two nodes—one on each side of the

elastic axis. From Fig. 1 it can be seen that the nodal points lie outside of the range between the c.g. and elastic axis for all values of ζ_1 and for values of ζ_2 numerically greater than L/r. For any given value of L/r, ζ_2 decreases numerically as ω_α/ω_h increases. Thus, the smallest possible numerical value of ζ_2 is obtained when ω_α/ω_h approaches infinity. Eq. (7) may be written

$$\zeta_2 = \frac{(\omega_\alpha/\omega_h)^2 - 1}{2L/r}\left\{1 - \sqrt{1 + 4\,\frac{(\omega_\alpha/\omega_h)^2(L/r)^2}{[(\omega_\alpha/\omega_h)^2 - 1]^2}}\right\}$$

As (ω_α/ω_h) becomes very large $(\omega_\alpha/\omega_h)^2 - 1$ approaches $(\omega_\alpha/\omega_h)^2$. Expanding by the binomial theorem and retaining only infinitesimals of the first order, the expression for ζ_2 may be written

$$\frac{(\omega_\alpha/\omega_h)^2}{2L/r}\left\{1 - \left[1 + 2\left(\frac{L/r}{\omega_\alpha/\omega_h}\right)^2\right]\right\}$$

Finally

$$\lim_{\zeta_{2(\omega_\alpha/\omega_h)} \to \infty} = -L/r \tag{9}$$

Therefore the negative root can never be numerically less than L/r. Thus it can be seen that the nodal points can never lie between the c.g. and the elastic axis.

Again from Eq. (7)

$$\zeta_1\zeta_2 = -(\omega_\alpha/\omega_h)^2 \tag{10}$$

In order to identify the corresponding values of ζ and ω, Eq. (5) may be written

$$(\Omega/\omega_h)^2 = \zeta/(\zeta + L/r) \tag{11}$$

By inspection of Eqs. (9) and (11) it can be seen that $\zeta/(\zeta + L/r)$ is always positive. Further, from Eq. (11), $(\Omega/\omega_h)^2$ is greater than unity for all negative values of ζ and less than unity for all positive values. Thus the positive root of Eq. (7) is always associated with the smaller value of Ω and vice versa. Alternatively, it may be said that the larger coupled frequency Ω_2 always occurs about a node that lies on the same side of the elastic axis as the c.g. Conversely, the c.g. and the node for the lower frequency Ω_1 lie on opposite sides of the elastic axis. Eq. (7) has been presented graphically in Figs. 2a and 2b.

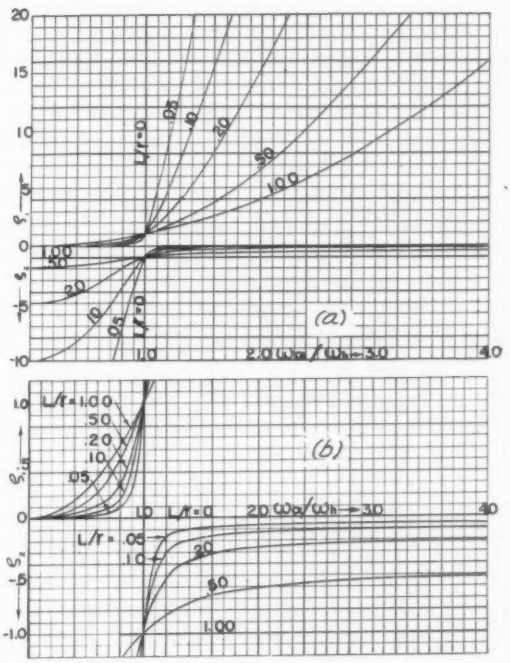

FIG. 2. Location of nodal points at resonance. (For reference see Eq. (7).) *Note:* (a) and (b) are identical except for the scale of ζ.

The foregoing discussion has applied only to the nodes that occur during free vibrations at resonance. Eqs. (3) and (4) may be solved to find h_0 and $r\alpha_0$. The quotient of these solutions $h_0/r\alpha_0$ is equal to ζ, from which the general solution for the nodal point in response to an applied force of any frequency ω is found to be

$$\zeta = \{[\omega^2 - \omega_\alpha{}^2/(\xi L/r + 1)]/[\omega^2 - \xi\omega_h{}^2/(L/r + \xi)]\}\{[\xi(L/r) + 1]/[(L/r) + \xi]\} \tag{12}$$

From Eq. (12) it can be seen that during forced vibrations ζ becomes independent of the applied frequency ω if

$$\omega_\alpha{}^2/[\xi(L/r) + 1] = \xi\omega_h{}^2/[(L/r) + \xi] \tag{13}$$

Eq. (13) may be solved for ξ, hence

$$\xi = \frac{[(\omega_\alpha/\omega_h)^2 - 1] \pm \sqrt{[(\omega_\alpha/\omega_h)^2 - 1]^2 + 4(\omega_\alpha/\omega_h)^2(L/r)^2}}{2L/r} \tag{14}$$

Comparison of Eqs. (7) and (14), which give identical expressions for ξ and ζ, shows that when the vibrator is placed at one node the point about which resultant rotation occurs is independent of the applied frequency and must be coincident with the other node.

Inspection of Eq. (8) shows that, as far as the coupled frequency Ω is concerned, ω_α and ω_h are interchangeable.

For this reason the uncoupled frequencies should be replaced by ω_g and ω_s, where the subscripts indicate "large" and "small" instead of "torsion" and "bending." Making these substitutions in Eq. (8) it is found that

$$\Omega_g^2 + \Omega_s^2 = (\omega_g^2 + \omega_s^2)/(1 - L^2/r^2) \tag{15}$$

$$\Omega_g^2\Omega_s^2 = \omega_g^2\omega_s^2/(1 - L^2/r^2) \tag{16}$$

From Eqs. (15) and (16) it is found that

$$(\omega_g/\Omega_g)^2 = \frac{(1 - L^2/r^2)(1 + \Omega_s^2/\Omega_g^2) + \sqrt{(1 - L^2/r^2)^2(1 + \Omega_s^2/\Omega_g^2)^2 - 4(1 - L^2/r^2)\Omega_s^2/\Omega_g^2}}{2} \tag{17}$$

$$(\omega_s/\Omega_s)^2 = \frac{(1 - L^2/r^2)(1 + \Omega_g^2/\Omega_s^2) - \sqrt{(1 - L^2/r^2)^2(1 + \Omega_g^2/\Omega_s^2)^2 - 4(1 - L^2/r^2)\Omega_g^2/\Omega_s^2}}{2} \tag{18}$$

These equations have been presented in graphic form in Fig. 3, from which the uncoupled frequencies may be found corresponding to any known values of L/r and the coupled frequency ratio Ω_s/Ω_g. It will be noted that the information given by Eqs. (17) and (18) is insufficient to determine which of the coupled frequencies is torsion about the elastic axis and which is bending. This is due to the fact that in Eq. (8) ω_α and ω_h are interchangeable. However, this is not true of Eq. (7), which can be used to establish the identity of the uncoupled frequencies. It can be seen that Eq. (7) would have been sufficient to find ω_α/ω_h directly if the values of ζ and L/r had been known. However, in vibration testing it is difficult to determine the nodal points with any degree of accuracy, whereas the measurement of frequency is quite straightforward. In this way it is most expedient to use Eq. (8) (or Fig. 3) to find the uncoupled frequencies, while a rough check between the observed nodes and those estimated by means of Eq. (7) (or Figs. 2a and 2b) will usually remove all ambiguity as to the identity of ω_α and ω_h.

The previous discussion refers strictly to a body vibrating in a vacuum. The equations of motion for a flat plate vibrating in the atmosphere have been derived by Theodorsen.[3] At zero air speed and assuming the control surface to be rigid, the solution of Eqs. (A) and (C) on page 10 of reference 3 reduces to the form

$$\Omega^4\left(1 - \left\{\frac{x_\alpha^2}{r_\alpha^2}\right\}\left\{\frac{(1 - a\kappa/x_\alpha)^2}{(1 + \kappa)[1 + \kappa(1/8 + a^2)/r_\alpha^2]}\right\}\right) - \Omega^2\left\{\frac{\omega_h^2}{(1 + \kappa)} + \frac{\omega_\alpha^2}{[1 + \kappa(1/8 + a^2)/r_\alpha^2]}\right\} + \left\{\frac{\omega_h^2}{(1 + \kappa)}\right\}\left\{\frac{\omega_\alpha^2}{[1 + \kappa(1/8 + a^2)/r_\alpha^2]}\right\} = 0 \tag{19}$$

Introducing the following parameters, which all become unity for $\kappa = 0$ (i.e., in a vacuum),

$$\mu^2 = (1 - a\kappa/x_\alpha)^2/\{(1 + \kappa)[1 + \kappa(1/8 + a^2)/r_\alpha^2]\}$$
$$\mu_\alpha^2 = 1/[1 + \kappa(1/8 + a^2)/r_\alpha^2]$$
$$\mu_h^2 = 1/(1 + \kappa)$$

Eq. (19) takes the form

$$\Omega^2 = \frac{[(\mu_\alpha\omega_\alpha)^2 + (\mu_h\omega_h)^2] \mp \sqrt{[(\mu_\alpha\omega_\alpha)^2 + (\mu_h\omega_h)^2]^2 - 4(\mu_\alpha\omega_\alpha)^2(\mu_h\omega_h)^2[1 - (\mu x_\alpha/r_\alpha)^2]}}{2[1 - (\mu x_\alpha/r_\alpha)^2]} \tag{20}$$

It can be seen that Eqs. (8) and (20) express exactly the same functional relationship if $(\mu x_\alpha/r_\alpha)$, $(\mu_\alpha\omega_\alpha)$ and $(\mu_h\omega_h)$ be substituted for (L/r), ω_α and ω_h, respectively. The parameters μ_α and μ_h cannot be arbitrarily associated with the greater and smaller frequencies as was done with ω_g and ω_s in Eqs. (17) and (18). However, the air mass correction can be applied only to bodies having the form of flat plates or airfoils; further, it may be said that for all conventional airfoil surfaces ω_α is greater than ω_h. Thus the solution for the uncoupled frequencies, as given by Eq. (20), has been determined in the form of Eqs. (17) and (18), except that it has been assumed that $\mu_\alpha\omega_\alpha$ is always greater than $\mu_h\omega_h$. These results have been plotted in Fig. 4.

Application to Three-Dimensional Structures

All modes of vibration exhibited by an airplane are functions of the overall elastic and inertia characteristics of the structure. For the sake of simplicity, it is common practice to consider the major components separately—for example, a wing, an engine mount, the tail unit, etc. Provided that the mass and stiffness of each component is relatively small compared to that of the whole airplane, this assumption is well justified. Even so, a complete analysis of each three-dimensional component is usually complicated and may be replaced by a two-dimensional system. The choice of the equivalent system depends entirely upon the ingenuity of the designer; however, several commonly used examples will be discussed.

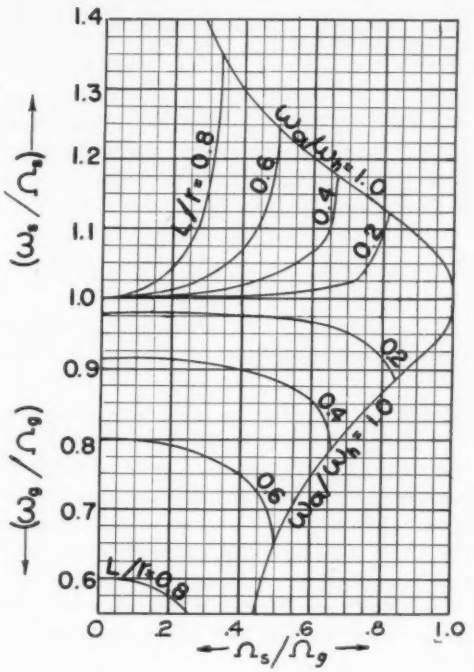

FIG. 3. Uncoupled frequencies in a vacuum. (For reference see Eqs. (17) and (18).)

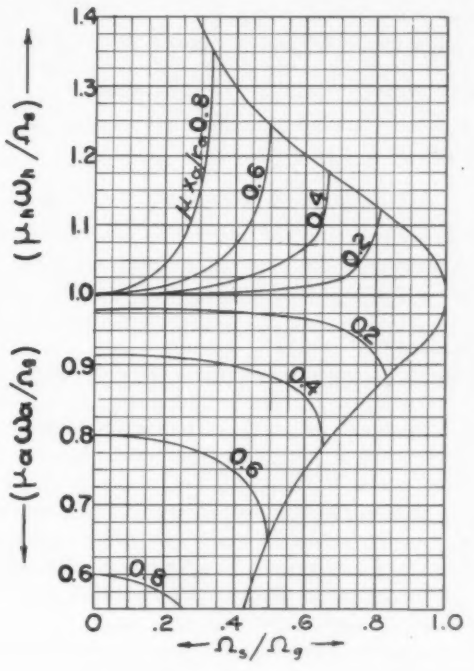

FIG. 4. Uncoupled frequencies in air. (For reference see Eq. (20).)

Wings

The equivalent weight may be taken as one-sixth of the entire weight of both wings and center section or, alternatively, as the weight of the outer half of one panel. The latter choice is better but frequently cannot be easily obtained.

The equivalent radius of gyration, c.g. and elastic axis locations may be taken to be identical with those of a section chosen three-fourths of the semispan from the centerline of the airplane.

The amplitudes of the equivalent system will also correspond to those of the actual wing at this reference section. Roughly speaking it may be said that the tip amplitude is twice the amplitude of the equivalent system—i.e., of the reference section.

Tail Units

With respect to fuselage torsion and side bending, the entire tail unit may be considered as a rigid body, its weight, c.g. location and radius of gyration being used directly in the equivalent system. The actual elastic axis of the fuselage determined at the rudder hinge station supplies the remaining parameter.

Engine Installations

The engine itself may be considered as the rigid body. Provided that one of the principal elastic axes of the mounting structure is nearly parallel to the thrust line, it may be used in the equivalent system. If, however, it is not approximately parallel, this problem must be given special consideration.

Application to Flutter Analysis

In the fundamental flutter theory, the following parameters, as defined by Theodorsen,[4] are of primary importance: ω_h = uncoupled circular bending frequency (rad. per sec.) and ω_α = uncoupled circular torsional frequency about the elastic axis (rad. per sec.). These parameters may be calculated, but more often they are determined by means of vibration tests on the finished airplane. Frequently, the observed coupled frequencies are substituted directly for ω_h and ω_α. In general, the elastic axis and c.g. of a wing are not coincident. For this reason the observed coupled frequencies are not identical with the desired uncoupled frequencies, as shown in Eq. (8). In many cases the error involved is not great, but, as the coupling factor L/r increases or the uncoupled frequency ratio approaches unity, the discrepancy becomes of increasing importance. For the purpose of analyzing vibration tests Eq. (8) has been written in the form of Eqs. (17) and (18). These have been plotted in Fig. 3, by means of which the uncoupled frequencies may be immediately determined from the observed values of Ω_g and Ω_s and the calculated value of L/r. It must be noted that L/r is numerically equal to x_α/r_α, as defined by Theodorsen in his flutter theory.[4] The effect of the surrounding atmosphere may be taken into account concurrently with the

correction for coupling by means of Eq. (20). The solution has been plotted in Fig. 4.

It must be noted that all parameters required for these transformations must be found in any case during a routine flutter analysis. Consequently, the additional work entailed by these corrections is quite negligible.

Application to Vibration Testing

There are two principal purposes of vibration testing: (1) to determine the resonant frequencies of the test specimen in its fundamental modes and (2) to determine the position of the nodal points corresponding to the fundamental modes.

Difficulty is encountered under the following conditions: (a) When the coupled frequency ratio is near unity it becomes difficult to distinguish between the two modes and, in particular, the nodal points become indistinct due to the superposition of one mode on the other. This condition is not uncommon with respect to fuselage bending and torsion. (b) When extraneous responses (e.g., skin panel buckling or harmonics) occur, the identification of the fundamental modes sometimes presents quite a problem.

In case (a) the problem of separating the two fundamental modes may be greatly simplified by placing the vibrator at one node. When this has been done, only vibrations about the other node can be excited, as shown by Eqs. (7) and (14); in this way each mode can be investigated separately without interference from the other. The Curtiss-Wright Universal Vibrator, as will be described later, is particularly well adapted to making use of this phenomenon.

In case (b) the extraneous responses may have widely differing characteristics. At times there is no doubt about their identification, while at others they become most confusing. In either event the observer can rely on his experience and judgment to make the proper choice. A careful comparison between the observed motions and the anticipated characteristics as indicated by Figs. 2a and 2b will often yield a definite answer to an otherwise ambiguous problem. Specific rules cannot be given because of the widely differing types of local responses that may be observed.

Even though a certain node may be well defined during a test, it is often extremely useful to have available some ready theoretic means of substantiating its position. That this is true can best be illustrated by means of an actual example. During the vibration tests of Airplane B (see "Numerical Example") the fuselage torsional node was distinctly observed to lie approximately 1 ft. below the tail cone. Because of the fact that the dynamic balance coefficient of the rudder had to be calculated with respect to this node, it was important that it should be observed correctly. A hearty discussion arose among the various observers, most of whom contended that it could not possibly lie outside of the fuselage and that probably the whole airplane was moving and therefore the node appeared in a fictitious position. The numerical result obtained by applying the methods of this paper to Airplane B shows clearly that not only was it possible for the node to lie outside the fuselage but also that the observed node was entirely correct. Had the information of Figs. 2 and 3 been available at the time of the test, the discussion might have reached an earlier and more rational conclusion.

Power and Unbalance Required for Vibration Tests

The choice and design of vibrators depend largely upon the three following items of fundamental importance:

(1) The power required to produce a given amplitude, the choice of the latter being a function of the available means by which it may be observed. When sensitive seismic-type pickups are used, an amplitude of only a few hundredths of an inch produces a measurable oscillation, while for direct visual observation about one-tenth of an inch total motion is necessary.

(2) The unbalance needed to absorb the required horsepower and, conversely, to produce the desired amplitude.

(3) The effect of airplane size upon the required power and unbalance.

It has been shown by Theodorsen[4] that the internal damping of a wing is in phase with the velocity during vibration, while its magnitude is proportional to the amplitude of the elastic restoring force. Neglecting the effect of air damping, which can be shown to be quite negligible at zero air speed, the following may be concluded (when $h = h_0 \sin \omega t$ and $\alpha = \alpha_0 \sin \omega t$):

Work done per cycle by internal damping

$$= 4 \int_0^{\pi/2} g_h C_h h_0 \cos \omega t \, dh + g_\alpha C_\alpha \alpha_0 \cos \omega t \, d\alpha \quad (21)$$

$$= 4(g_h C_h h_0^2 + g_\alpha C_\alpha \alpha_0^2) \int_0^{\pi/2} \cos^2 \omega t \, d(\omega t)$$

$$= (g_h C_h h_0^2 + g_\alpha C_\alpha \alpha_0^2)\pi \quad (22)$$

But

$$C_h = \omega_h^2 W/g$$

$$C_\alpha = r^2 \omega_\alpha^2 W/g$$

From Fig. 1 it can be seen that

$$h_0 = h_{10}(\zeta/X)$$

$$\alpha_0 = (h_{10}/X_\tau)$$

$$\text{Power} = \frac{\text{Work done per cycle by damping}}{\text{Time of one cycle}}$$

Therefore, making the above substitutions in Eq. (22)

$$P = {}^1/_2(W/g)h_{10}^2\omega^3[g_h(\omega_h/\omega)^2(\zeta/X)^2 + g_\alpha(\omega_\alpha/\omega)^2(1/X)^2] \quad (23)$$

The power absorbed by the vibrator will now be considered. Assuming sinusoidal motion

$$h_v = h_{v_0} \sin \omega t$$

$$F = F_0 \sin (\omega t + \phi) = (W_v r_v/g)\omega^2 \sin (\omega t + \phi)$$

Power absorbed by vibrator

$$= \int F \, dh_v/(2\pi/\omega)$$

$$= {}^1/_2(W_v r_v/g)\omega^3 h_{v_0} \sin \phi$$

At resonance $\phi = \pi/2$

$$P = {}^1/_2(W_v r_v/g)\omega^3 h_{v_0} \tag{24}$$

From Fig. 1

$$h_{v_0} = h_{10}(X_v/X)$$

Substituting in Eq. (24)

$$P = {}^1/_2(W_v r_v/g)\omega^3 h_{10}(X_v/X) \tag{25}$$

Eliminating P from Eqs. (23) and (25), rearranging and introducing the wing span B

$$W_v r_v/W h_{10} = (1/B\omega)^2(X/X_v)[g_h(B\omega_h)^2(\zeta/X)^2 + g_\alpha(B\omega_\alpha)^2(1/X)^2] \tag{26}$$

Comparison of Power Required for Bending and Torsion

Experience has shown that for conventional wings the torsional frequency is usually several times as great at that for bending. Thus, at bending resonance it can be seen from Figs. 2a and 2b that the nodal point lies several chord lengths ahead of the wing, while for torsion it lies near the mid chord point. The trailing edge will be assumed to be the observation point at which the amplitude h_{10} is measured. Then for all conventional wings the approximate values given in Table 1 may be used. Substituting the average values of Table 1 into Eq. (23), and assuming that $g_\alpha = g_h$, for bending (when $\omega \approx \omega_h$)

$$P = {}^1/_2(W/g)h_{10}{}^2\omega_h{}^3 g_h \, (0.81 + 0.05)$$

Therefore

$$P/h_{10}{}^2 \approx {}^1/_2(W/g)g_h\omega_h{}^3 \text{ (for all wings at bending resonance)} \tag{27}$$

Similarly, for torsion (when $\omega \approx \omega_\alpha$)

$$P = {}^1/_2(W/g)h_{10}{}^2 g_\alpha \omega_\alpha{}^3 \, (0.03 + 0.25)$$

Therefore

$$P/h_{10}{}^2 \approx {}^1/_2(W/g)g_\alpha\omega_\alpha{}^3/4 \text{ (for all wings at torsional resonance)} \tag{28}$$

A comparative study of Eqs. (27) and (28) shows that for the same trailing edge amplitude

$$\frac{P_{\text{(at torsional resonance)}}}{P_{\text{(at bending resonance)}}} \approx {}^1/_4(\omega_\alpha/\omega_h)^3$$

Since the frequency ratio of conventional wings usually lies between 2 and 4, it can be seen that the power required at torsional resonance is from two to sixteen times greater than that required to produce the same trailing edge amplitude in bending.

Table 1

Range of Values of Parameters for Conventional Wings

Parameters	Value at Bending Resonance	Value at Torsional Resonance
ζ/X	$0.8 \rightarrow 1.0$	$-0.3 \rightarrow -0.5$
$1/X$	$0.05 \rightarrow 0.10$	$0.4 \rightarrow 0.6$
ω_h/ω	1.0	$0.25 \rightarrow 0.50$
ω_α/ω	$2 \rightarrow 4$	1.0

From Eqs. (27) and (28) it can be seen that for a given amplitude, which is determined by the available measuring equipment, and for geometrically similar wings

$$P \propto W\omega^3 \propto (B\omega)^3$$

Experience has shown[5] that the resonant frequencies vary inversely as the span. Therefore, the power required to produce a given amplitude is roughly independent of airplane size.

It will be shown later by means of a numerical example (see Airplane A) that the theoretic power required to produce one-tenth of an inch motion at the trailing edge is 0.00064 and 0.0134 hp. at bending and torsional resonance, respectively. Since the actual power required to vibrate the wing is so small, it can be seen that the motor for the vibrator need only be designed to overcome the friction horsepower in the moving system.

A similar analysis of Eq. (26) shows that the required unbalance varies directly with the amplitude and with the weight of the surface being tested. Thus, for a given amplitude, the required unbalance must increase roughly as the cube of the wing span.

The foregoing analysis can be applied to a three-dimensional wing by means of the substitutions outlined under the heading "Application to Three-Dimensional Structures."

Note on Structural Damping

At the present time there is little quantitative information about the structural damping present in aircraft structures. A limited amount of experimental data has been summarized by Wylie.[7] The actual values of g_h and g_α depend upon the type of design and the material used. They vary from 0.04 to 0.09 for metal monoplanes, and usually $g_h \approx g_\alpha$. For purposes of numerical examples in this paper, the structural damping has been assumed to be 0.05 in all cases. It can be seen from Eqs. (23) and (26) that the power and unbalance required to produce a given amplitude both vary directly with the structural damping coefficients.

For a particular structure the damping coefficients may be evaluated from test results if the amplitude re-

sponse to a constant exciting force at different frequencies is observed. Then

$$g = (n_2^2 - n_1^2)/(n_2^2 + n_1^2)$$

where n_1 and n_2 are the two frequencies at which the observed response is equal to the maximum response divided by the square root of 2. The appropriate subscript must be supplied according to whether bending or torsional oscillations are observed. It must be noted that a constant applied force is specified. When a conventional unbalanced vibrator is used, all observed amplitudes must be divided by the square of the corresponding frequency before finding n_1 and n_2.

Numerical Example

Airplane A

Chord	= 4.71 ft.
r	= 1.48 ft.
x_α	= 0.36
r_α	= 0.63
Coupling factor $= L/r = x_\alpha/r_\alpha$	= 0.57
a	= − 0.40
κ	= 0.12
Weight of entire wing unit	= 730 lbs.
$W = 730/6$	= 122 lbs.
Measured bending frequency	= 580 c.p.m.
Measured torsional frequency	= 2,400 c.p.m.

(1) Determination of Uncoupled Wing Frequencies

$\Omega_z = (580)(2\pi/60)$ = 60.8 rad. per sec.
$\Omega_\theta = (2,400)(2\pi/60)$ = 251.2 rad. per sec.
Coupled frequency ratio $= \Omega_z/\Omega_\theta = 0.242$

$$\mu = \sqrt{\frac{[1 - (a\kappa/x_\alpha)]^2}{(1 + \kappa)\{1 + (\kappa/r_\alpha^2)(1/8 + a^2)\}}} = 1.026$$

$$\mu_\alpha = \sqrt{\frac{1}{1 + (\kappa/r_\alpha^2)(1/8 + a^2)}} = 0.960$$

$$\mu_h = \sqrt{1/(1 + \kappa)} = 0.945$$

From Fig. 3 (neglecting effect of air mass)

ω_z/Ω_z	= 1.016
$\omega_\theta/\Omega_\theta$	= 0.809

Because of the conventional nature of the wing vibration, it is quite evident that ω_α is associated with ω_θ and ω_h with ω_z, and there is no ambiguity.

Table 2
Example of Coupled and Uncoupled Frequencies

	Measured Frequency, c.p.m.	Uncoupled Frequencies— Air mass neglected, c.p.m.	Air mass corrected, c.p.m.
Bending	580	588	626
Torsion	2,400	1,940	1,995

$\omega_h = (1.016)(580)(2\pi/60) = (588)(2\pi/60)$ rad. per sec.
$\omega_\alpha = (0.809)(2,400)(2\pi/60) = (1,940)(2\pi/60)$ rad. per sec.

From Fig. 4 (including air mass correction)

$\mu x_\alpha/r_\alpha = (1.026)(0.57) = 0.585$
$\mu_h\omega_h/\Omega_z = 1.018$
$\mu_\alpha\omega_\alpha/\Omega_\theta = 0.798$
$\omega_h = 1.018\Omega_z/\mu_h = [(1.018)(580)/0.945]\,[2\pi/60]$
$= (626)(2\pi/60)$ rad. per sec.
$\omega_\alpha = 0.798\Omega_\theta/\mu_\alpha = [(0.798)(2,400)/0.960]\,[2\pi/60]$
$= (1,995)(2\pi/60)$ rad. per sec.

The results of the numerical example have been summarized in Table 2. Thus it can be seen that the effect of coupling is not negligible insofar as it allows nearly a 20 per cent error in the torsional frequency that should be used in the flutter calculations; this entails, roughly speaking, a 20 per cent unconservative error in the calculations of the bending-torsion flutter speed. The effect of air mass is considerably less, being in the order of 5 per cent for both, though somewhat greater for bending than torsion. Further, the neglect of the air mass correction leads to a conservative answer.

(2) Power and Unbalance Required to Vibrate Wing

From Table 2

$\omega_\alpha = (1,995)(2\pi/60) = 208.8$ rad. per sec.
$\omega_h = (626)(2\pi/60) = 65.6$ rad. per sec.
$\omega_\alpha/\omega_h = 3.18$

Therefore from Figs. 2a and 2b

$\zeta_1 = +16.0$
$\zeta_2 = -0.63$

The elastic axis is at 30 per cent of the chord from the leading edge.

With reference to Fig. 1 it can be seen that at bending resonance

$$Xr = \zeta_1 r + 0.7 \text{ (chord)}$$

$$X = 16 + [(0.7)(4.71)/1.48] = 18.2$$

$$\zeta_1/X = 0.88$$

Similarly, at torsional resonance

$$X = -0.63 + [(0.7)(4.71)/1.48] = 1.60$$

$$\zeta_2/X = -0.39$$

Assuming that $g_\alpha = g_h$ and substituting the appropriate values in Eq. (23), at bending resonance

$$P = h_{10}^2 g_h \times \frac{122}{32.2} \times \frac{60.8^3}{2}\left[\left(\frac{65.6}{60.8}\right)^2 (0.88)^2 + \left(\frac{208.8}{60.8}\right)^2\left(\frac{1}{18.2}\right)^2\right] = h_{10}^2 g_h \times 0.40 \times 10^6 \quad (29)$$

At torsional resonance

$$P = h_{10}^2 g_\alpha \times \frac{122}{32.2} \times \frac{251.2^3}{2}\left[\left(\frac{65.6}{251.2}\right)^2 (-0.39)^2 + \left(\frac{208.8}{251.2}\right)^2\left(\frac{1}{1.60}\right)^2\right] = h_{10}^2 g_\alpha \times 8.3 \times 10^6 \quad (30)$$

With reference to these numerical operations it can be seen that the power required for bending depends almost entirely upon the first term in parentheses, while that for torsion is controlled by the second term. Eqs. (29) and (30) show that the power required is 20 times greater for torsion than for bending if the trailing edge amplitude is to be the same in both cases.

In order to estimate the required unbalance, it shall be assumed that the vibrator is located on the trailing edge, in which case $X_v/X = 1$. Making the appropriate substitutions in Eq. (26) and canceling out the span B (since the actual frequencies are known), at bending resonance

$$W_v r_v / W h_{10} = g_h \times 0.937 \quad (31)$$

At torsional resonance

$$W_v r_v / W h_{10} = g_\alpha \times 0.280 \quad (32)$$

The power and unbalance required to produce one-tenth of an inch total motion at the trailing edge will be determined.

$$h_{10} = 0.05/12 = 0.0042 \text{ ft.}$$

Substituting in Eqs. (29), (30), (31), and (32) and assuming that $g_\alpha = g_h = 0.05$

$$\text{Horsepower} = \frac{(0.0042)^2 \times 0.05 \times 0.40 \times 10^6}{550}$$

$$= 0.00064 \text{ hp. (at bending resonance)}$$

$$\text{Horsepower} = 0.0134 \text{ hp. (at torsional resonance)}$$

$$\text{Unbalance} = W_v r_v = 122 \times 0.0042 \times 0.05 \times 0.937 \times 12 = 0.288 \text{ lb.in. (at bending resonance)}$$

$$\text{Unbalance} = 0.086 \text{ lb.in. (at torsional resonance)}$$

The numerical values obtained for the horsepower required are roughly representative of all airplanes similar in size and general design to the one chosen. This is not true, however, with regard to the unbalance required; in this case the location of the vibrator has such a large effect that each particular location must be investigated separately.

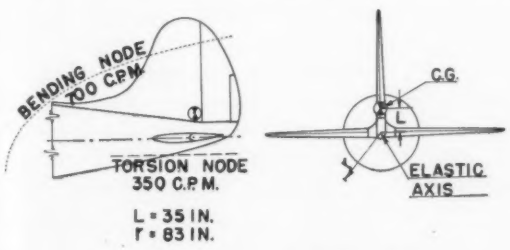

FIG. 5. Tail unit of airplane B.

Airplane B (Analysis of fuselage vibrations)

Vibrations involving torsion and side bending of the fuselage shall be considered. The tail end of this airplane is shown diagrammatically in Fig. 5.

$$L = 35 \text{ in. (estimated)}$$
$$r = 83 \text{ in. (estimated)}$$
$$\text{Coupling factor } L/r = 0.42$$
$$\text{Side bending frequency (measured)} = 700 \text{ c.p.m.}$$
$$\text{Torsional frequency (measured)} = 350 \text{ c.p.m.}$$

From Fig. 3

$$\omega_s/\Omega_s = 1.05$$
$$\omega_g/\Omega_g = 0.88$$
$$\omega_s/\omega_g = \frac{1.05}{0.88} \times \frac{350}{700} = 0.60$$

It is now known that the uncoupled frequency ratio is 0.60, but it is uncertain where ω_α or ω_h is the larger.

With reference to Figs. 2a and 2b, assuming

$$\omega_\alpha/\omega_h = 1/0.60 = 1.7$$
$$\zeta_1 = +5.5$$
$$\zeta_2 = -0.57$$

The nodal points are given by ζr—i.e., 460 in. below the elastic axis and 47 in. above the elastic axis. These do not agree with observed results. Therefore it shall be assumed that

$$\omega_\alpha/\omega_h = 0.60$$

from Figs. 2a and 2b

$$\zeta_1 = 0.20$$
$$\zeta_2 = -1.8$$

Hence, the nodal points are 17 in. below elastic axis and 150 in. above elastic axis. These agree with the observed results as discussed after Eq. (18) and also at the end of the discussion on "Application to Vibration Testing."

CURTISS-WRIGHT UNIVERSAL VIBRATOR

The vibrator is illustrated diagrammatically in Fig. 6, while photographs are shown in Figs. 7 and 8. Fundamentally it consists of two unbalanced rotors mounted on parallel shafts 20 in. apart. They are driven in the same direction by means of bevel gears mounted on a stiff aluminum alloy torque tube. In this way the natural frequency of the system is above the highest speed for which the vibrator has been designed to operate (viz., 2,500 c.p.m.). The rotors may be connected so that they are in phase (i.e., so that centrifugal forces act in same direction) or 180 deg. out of phase as shown in Fig. 6. In either case the combination can be replaced by a single equivalent rotor at a point R, as shown in Fig. 6b. When the rotors are in phase,

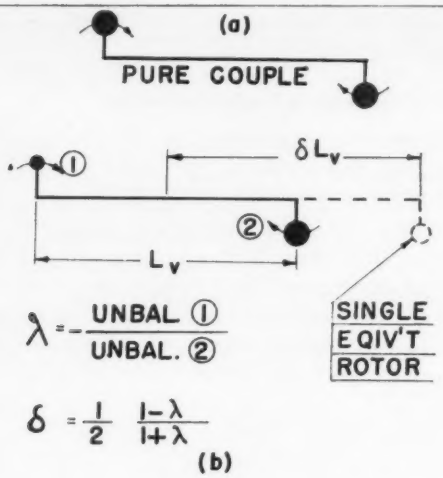

FIG. 6. Curtiss-Wright Universal Vibrator (diagrammatic).

R lies between them and the equivalent unbalance is equal to the sum of the actual unbalances; when the rotors are 180 deg. out of phase, R lies to one side as shown in Fig. 6b and the equivalent unbalance is equal to the difference between the unbalances of the actual rotors. The location of R with respect to the centerline of the system is defined by δL_v, where L_v is the distance between rotors. The parameter δ is given by the equation

$$\delta = {}^1/_2(1 - \lambda)/(1 + \lambda) \qquad (33)$$

where λ is the ratio of the smaller to the larger rotor unbalance. When the rotors are in phase, λ is positive; when 180 deg. out of phase, λ is negative. From Eq. (33) it can be seen that the single equivalent rotor may be made to act at any point along the line joining the two actual rotors. In the limit, when the rotors are equal and $\lambda = -1$, the equivalent rotor becomes infinitely small and is located at infinity. In this way a pure couple is applied by the vibrator, which is particularly effective for the purpose of exciting torsional oscillations.

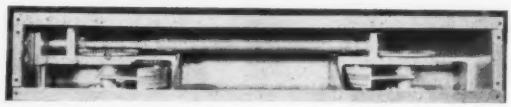

FIG. 7. Curtiss-Wright Universal Vibrator.

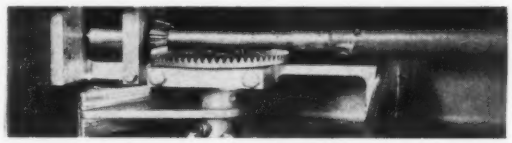

FIG. 8. Detail of rotor.

In order to make use of the phenomenon illustrated by Eq. (33), the unbalanced weight on each rotor is built up by means of eight separate sectors cut from ${}^1/_8$-in. steel sheet. In this way the unbalance of each rotor may be varied from 1 to 7 lb.in. As explained previously this feature can be used to advantage in isolating obscure modes.

REFERENCES

[1] Den Hartog, J. P., *Mechanical Vibrations*, Second Edition, p. 102; McGraw-Hill Book Co., Inc., New York, 1940.

[2] Timoshenko, S., *Vibration Problems in Engineering*, Second Edition, p. 232; D. Van Nostrand Co., Inc., New York, 1937.

[3] Theodorsen, Theodore, *General Theory of Aerodynamic Instability and the Mechanism of Flutter*, N.A.C.A. T.R. No. 496, 1935.

[4] Theodorsen, Theodore, and Garrick, I. E., *Mechanism of Flutter. A Theoretical and Experimental Investigation of the Flutter Problem*, N.A.C.A. T.R. No. 685, 1940.

[5] Lombard, A. E., *Flutter in Aircraft*, Thesis in partial fulfillment of the Degree of Doctor of Philosophy, California Institute of Technology, Pasadena, Calif., 1939 (unpublished).

[6] Kassner, R., and Fingado, H., *The Two-Dimensional Problem of Wing Vibration*, Journal of the Royal Aeronautical Society, Vol. 41, pp. 921–944, October, 1937; translated from Luftfahrtforschung, Vol. 13, No. 11, pp. 374–387, November 20, 1936.

[7] Wylie, Jean, *Perpendicular Axes Control Surface Binary Flutter*, p. 134; Civil Aeronautics Administration. Certificate and Inspection Release No. 46, Aircraft Airworthiness Section Report No. 23, April, 1941.

Determination of Airplane Critical Altitude by Flight Tests

L. C. MILLER*

Brewster Aeronautical Corporation

SUMMARY

The determination of airplane critical altitude has become of considerable importance during the last four or five years. The method presented in this paper has been developed around a practical problem on a specific airplane. By use of this method it has been possible to establish the high speed of a type airplane so that it may be checked from flights of other airplanes of the type and under varying atmospheric conditions. The problem applies to an installation using a two-speed single-stage mechanical supercharger. The problem becomes more complicated when two-stage supercharging and exhaust turbosupercharging are used. Some of the factors relating to the latter type of installation are indicated.

The particular benefit gained from the determination of airplane critical altitude is the establishment of the airplane high speed and the establishment of the increase of high speed effected by careful design of the carburetor air scoop for the attainment of the highest possible ram due to the dynamic pressure of the air entering the carburetor scoop.

INTRODUCTION

WITH THE ADVENT OF AIRPLANES that exceeded a maximum speed of 300 m.p.h., there came a realization that the ramming effect of air in the carburetor air scoop, due to dynamic pressure, caused the engine b.hp. to be increased by an amount sufficient to increase substantially the airplane speed.

This characteristic assumed the nature of something obtained for nothing and, as the value of each mile per hour added to the high speed is placed high in seeking supremacy in military aircraft design, aircraft manufacturers have commenced to pay more attention to the effect of ram. The method to be described in this paper is the result of actually working out a check of the ram effect in increasing the altitude at which the rated horsepower of the engine can be obtained.

Critical altitude will vary depending upon the power-operating condition of the engine—i.e., high speed in level flight, climb, cruising, etc. The gain is most significant in the high-speed operating condition. The present discussion is therefore limited to the critical altitude for high speed when maximum rated power is obtained from the engine in level flight.

The problem becomes one of engine-operating characteristics to a large degree. However, since the airplane manufacturer designs and installs the carburetor air scoop, which is responsible for the increased altitude of operation, and since the actual result must be determined by flight tests of the finished airplane, it becomes the responsibility of the airplane manufacturer to obtain the desired results. In the present instance, the need to rely on the engine manufacturer for cooperation in solving the combined design and flight test problem met with ready response from the Field Engineering Division of the engine manufacturer. As a result, this method for actually determining airplane critical altitude has been prepared.

Received November 6, 1941.

* Now associated with Wright Aeronautical Corporation Division Curtiss-Wright Corporation.

DEFINITIONS

To clarify some of the terms characteristic of this problem the following definitions are given:

(1) Ram is the increment of pressure present at the carburetor top deck, due to the effect of dynamic pressure of the air at the entrance to the carburetor air intake scoop. Ram is often measured in feet of altitude. The value so stated is the equivalent to the aforementioned increment of pressure under standard atmospheric conditions.

(2) Critical altitude, in general, may be defined as the highest altitude in standard atmosphere at which the rated b.hp. of the engine is developed.

(3) Engine critical altitude is the highest altitude in standard atmosphere at which the engine, if operated without carburetor temperature rise or ram, would deliver its rated b.hp. at its rated r.p.m.

(4) Airplane critical altitude is the highest altitude in standard atmosphere at which the engine, as installed and as effected by ram and carburetor air temperature rise, will deliver its rated b.hp. at its rated r.p.m.

(5) Supercharger compression ratio is the ratio of the manifold pressure to the carburetor top deck pressure. The manifold pressure is the pressure aft of the supercharger blower and before entering the cylinders. Carburetor top deck pressure is the pressure of the charge of air at the carburetor entrance.

EFFECT OF PREVAILING ATMOSPHERIC CONDITIONS

Engines are rated for a limited b.hp. and r.p.m. up to the maximum altitude at which the b.hp. can be delivered. The rated b.hp. is determined by the physical and strength characteristics of the materials used in the engine consistent with satisfactory length of service. The highest altitude at which rated power can be ob-

tained is the altitude at which, because of supercharging by an internal or exhaust-driven blower, the necessary weight flow of air can be maintained to the engine. This altitude is called the engine critical altitude if the engine is operated without carburetor air temperature rise or ram.

The dynamic pressure of the air entering the intake scoop may add to the pressure at the carburetor top deck. Now, since added carburetor pressure above normal atmospheric pressure is available at the rated altitude of the engine because of ram on the carburetor air scoop, more than rated b.hp. is available from the engine; or if the b.hp. is limited to its rated value, the full inherent pumping capacity of the engine is not used. This balance of the engine pumping power is therefore available at higher altitudes to permit obtaining rated b.hp., where, without the added effect of ram, the rated b.hp. could not have been obtained.

The highest altitude at which the added pressure due to ram is effective is airplane critical altitude, as previously defined, and depends upon the aerodynamic efficiency of the air intake scoop to the carburetor.

While ram effect of the air in the carburetor scoop adds to the power, carburetor air temperature rise detracts from the power, so that the net gain due to ducting the air to the carburetor is the resultant of the two effects.

Airplane critical altitude differs from engine critical altitude because ram depends on the design of the engine cowling and carburetor air intake, and only a part of the total available energy of the air attributable to ram is available at best and a rise in carburetor air temperature occurs in the intake duct. If a stated amount of ram could definitely be obtained in any airplane it would still be necessary to correct for carburetor air temperature rise.

Airplane critical altitude is significant to an airplane in that its maximum speed will be obtained at the highest altitude that the rated power can be obtained.

Rated b.hp. produced at the higher altitude due to ram usually allows a higher speed because of the lower air density at the higher altitude.

Actual airplane critical altitude can only be obtained from flight tests where measurements of carburetor ram under flight conditions will determine the efficiency with which the carburetor scoop has been designed for producing ram.

Since standard conditions are rarely met when flight tests are made and since the variant factors affect the horsepower produced, as well as the aerodynamic drag and lift of the airplane, it is necessary to be able to correct engine b.hp. from observed atmospheric temperature and pressure conditions to standard conditions before the actual altitude at which rated b.hp. can be obtained under standard conditions, or better the critical altitude, can be determined. Once it is known at what altitude rated b.hp. is obtainable, it is possible to determine the high speed of the airplane with rated b.hp.

Description of Method

A method for determining airplane critical altitude from flight test observations follows. The determination of critical altitude by this method is carried out by showing the effect of the deviations from standard conditions on the power calibration curve (Fig. 1).

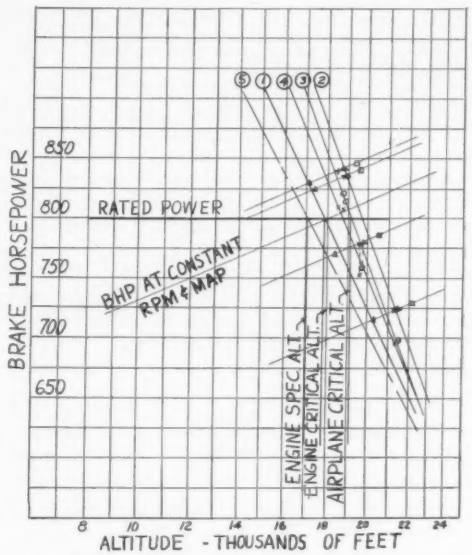

Fig. 1. Engine power curves corrected for ram and carburetor air temperature. Brewster model 339, Wright R-1820-G105A. 1, Zero ram, zero carburetor rise. 2, Actual ram, uncorrected b.hp. 3, Actual ram and carburetor rise. 4, Observed data. 5, Specified b.hp. vs. altitude.

The method as outlined here applies to a two-speed mechanically driven supercharged air-cooled engine on a single-engine tractor airplane. The observed data are taken from a chosen pressure altitude. Since the pressure altitude is observed, only temperature corrections need be made to b.hp. and intake air to correct to standard conditions of altitude.

The required data are obtained by flying the airplane at full throttle with best power mixture setting at several altitudes near the expected critical altitude, making b.hp. and r.p.m. measurements by means of a torquemeter and tachometer and observing sufficient atmospheric data that corrections may be made to standard conditions. When altitudes, corrected for the effect of ram and carburetor temperature rise, are plotted on the line of constant r.p.m. and m.a.p. (manifold absolute pressure) against b.hp. corrected for carburetor temperature rise, the intersection of the rated b.hp. line at rated r.p.m. with altitude on this curve is the engine critical altitude. In the process of developing the corrected b.hp. curve against altitude, the observed b.hp. values are plotted against altitude. Corrections for deviations from standard conditions of temperature are made on the power curve sheet by finding the new b.hp. under constant conditions of r.p.m. and manifold pressure at altitudes represented by the

known pressure variations due to the deviations from standard conditions.

Fig. 1 illustrates the differences between engine critical altitude, observed airplane critical altitude and corrected airplane critical altitude. Curve 1 shows the engine power corrected to standard atmosphere if there were no ram and no carburetor temperature rise. Curve 2 shows the result of correcting power curve 1 for the effect of ram. The correction of b.hp. for carburetor temperature rise is not yet applied on this curve, and the curve only represents a step in the process of solving the problem. Curve 3 shows the correction of b.hp. of curve 2 to actual carburetor temperature rise, and, hence, represents the true airplane critical altitude condition. Curve 4 shows the engine power as obtained from observed data and not corrected for deviations from standard atmosphere. Curve 5 shows the engine rated b.hp. against altitude as plotted from the engine manufacturer's calibration of the engine.

Outline of Method

Insofar as a definite carburetor temperature rise is inherent in the installation, the calculation has been figured on the basis of this temperature rise existing under otherwise standard conditions. A curve of actual carburetor air temperature rise against outside air temperature is plotted on Fig. 2. (These data are observed data for the particular airplane installation being investigated.)

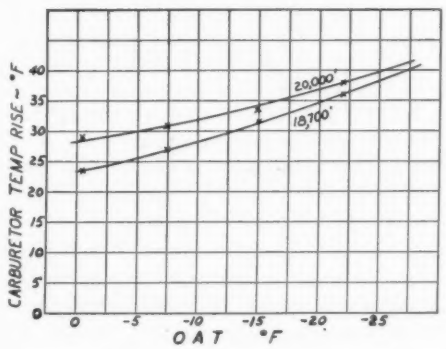

Fig. 2. Full throttle carburetor air temperature rise. Observed data.

During a flight test for determining critical altitude, the following data should be observed under maximum rated power operating conditions in level flight: (1) r.p.m., (2) manifold pressure, (3) carburetor ram, (4) outside air temperature, (5) carburetor air temperature, (6) pressure altitude, and (7) torquemeter reading for b.hp.

The calculations to be made from the observed data are as follows: (1) Determine the standard altitude pressure for the several observed sets of data by dividing observed manifold pressure by the supercharger compression ratio for the following conditions: (a) Observed altitude pressure plus observed ram corrected to zero carburetor air temperature rise and, by dividing the observed manifold pressure by this corrected supercharger compression ratio, obtain the corrected standard altitude pressure. (b) Corrected standard altitude pressure of condition 1(a) minus ram and corrected to include actual carburetor air temperature rise.

(2) Determine the equivalent standard altitude represented in the carburetor top deck for the pressures obtained in 1(a) and 1(b).

Pressure of step 1(a) gives the standard altitude that would give the same performance as the observed performance if no ram or carburetor temperature rise existed for the same carburetor top deck pressure. These altitudes plotted against observed b.hp. would give the power curve for zero ram and zero carburetor temperature rise condition. From this curve, engine critical altitude can be obtained. Pressure from the condition of 1(b) gives standard altitudes that give the same performance as if ram and actual carburetor temperature rise were added. These altitudes plotted against b.hp. corrected for actual carburetor air temperature rise give the power curve for the airplane operating condition.

The curve of 1(a) is plotted directly from computations. The curve of 1(b) is obtained as follows: Correct the altitudes of step 1(a) to standard altitudes that would exist when ram and actual carburetor air temperature rise are present. This is obtained by deducting ram from the carburetor top deck pressures and correcting the supercharger compression ratio for actual carburetor temperature rise over temperature of step 1(a) and finding the corresponding standard altitudes.

Plot these altitudes on the constant r.p.m. and manifold pressure lines of the power curves of Fig. 1 and draw the resulting power curve. This gives a power curve for actual ram and with actual carburetor temperature condition.

The b.hp. on this last curve must now be reduced to correct for the effect of increase in carburetor temperature on b.hp. itself. These corrections are made by correcting b.hp. to 0° carburetor temperature rise by the formula

$$\text{b.hp.}_c = \text{b.hp.}_o \sqrt{\text{t.c.a.}/\text{t.f.a.}}$$

where

b.hp._c = corrected brake horsepower
b.hp._o = observed brake horsepower
t.c.a. = absolute temperature of the carburetor air
t.f.a. = absolute temperature of free air at standard altitude conditions

Values of carburetor temperature rise are obtained from Fig. 2.

This last power curve is the curve of step 1(b). The altitude at which rated b.hp. occurs on this curve is the airplane critical altitude. This, as stated previously,

is the highest altitude under standard atmospheric conditions at which rated b.hp. would be obtained for the ram and carburetor air temperature rise conditions existent.

The steps for carrying out the above procedures are as follows:

(1) Note pressure altitude as read on the sensitive altimeter in feet.

(2) Note the r.p.m. as set on the propeller control and maintained constant by governing.

(3) Read the manifold pressure called for on the engine calibration curves at the selected pressure altitude.

(4) Determine the ram, which is the measured increase in pressure in inches of water in the carburetor air scoop over the actual outside pressure for the operating condition.

(5) Note the carburetor air temperature observed on a thermometer in °F.—i.e., the temperature of the air at the carburetor top deck.

(6) Note outside air temperature in °F. in the free air stream at the selected pressure altitude.

(7) Compute b.hp. from torquemeter and tachometer readings.

(8) Standard air temperature.

(9) Correct b.hp. to 0° carburetor air temperature rise.

(10) Convert the ram of 4 to inches of mercury.

(11) Find the pressure that corresponds to the observed pressure altitude from the standard atmosphere tables.

(12) Combine 10 and 11 to get the pressure at the carburetor top deck.

(13) The compression ratio of the supercharger is obtained by dividing manifold pressure 3 by the carburetor top deck pressure 12. The manifold pressure is the pressure aft of the blower and the carburetor inlet pressure is the pressure before the blower.

(14) The compression ratio 13 must be corrected now for temperature variation of the carburetor air temperature from outside air temperature of a standard day. This is a function of the engine as plotted on Wright Aeronautical Corporation Curve No. 1693 (Fig. 3).

(15) Having now obtained the corrected compression ratio as affected by deviation from carburetor air temperature, it is divided into the manifold pressure 3 to determine the standard pressure equivalent to the conditions as they were observed.

(16) The altitude is now found from the standard altitude charts corresponding to 15. This altitude is the altitude that under the observed conditions would have been obtained if there were no ram and no deviations from standard pressure.

(17) Plot the altitudes 16 on constant r.p.m.-m.a.p. line from b.hp. 9. The intersection of this curve with the rated b.hp. of the engine gives the engine critical altitude.

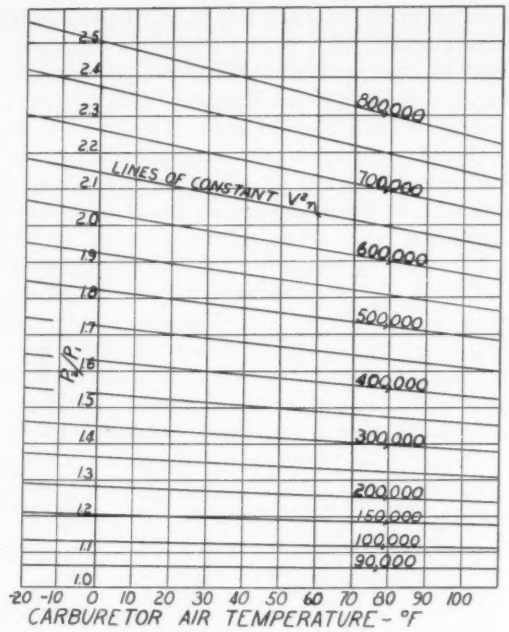

FIG. 3. The ratio of pressure at blower outlet to pressure at impeller inlet as a function of carburetor air temperature is P_2/P_1. W.A.C. curve No. 1693. Formulas: $P_2/P_1 = (y + 1)^{3.53}$, $y = v^2m/5960Tk$, where $n = 0.67$.

(18) Subtract the ram in inches of Hg from the standard altitude pressure 15.

(19) Determine the standard altitude represented by the standard pressures 18.

(20) Find the carburetor air temperature °F. at the altitude 19 from Fig. 2.

(21) Correct the compression ratio 14 for the carburetor air temperature 20.

(22) Find the standard altitude pressure for the corrected compression ratio 21 by dividing the pressure ratio into the manifold pressure 3.

(23) Subtract the pressure due to ram from the pressure 22. This gives the pressure representing the standard altitude that would prevail if there were ram and actual carburetor temperature rise.

(24) Find the altitudes obtained from pressures 23 and plot on lines for variation of b.hp. versus altitude as constant r.p.m. and manifold pressure on Fig. 1. This curve represents the b.hp. uncorrected for carburetor temperature rise at the correct altitudes.

(25) List b.hp. at altitudes 24 from Curve 2 on Fig. 1.

(26) List standard temperature of altitudes 24.

(27) List carburetor air temperatures from Fig. 2 for altitudes 24 with temperatures in absolute degrees.

(28) Correct b.hp.$_c$ = b.hp.$_o$ $\sqrt{\text{t.c.a./t.f.a.}}$

(29) List corrected b.hp. and plot against altitudes 24.

(30) Where rated b.hp. intersects curve 29 is the airplane critical altitude.

TABLE 1
Sample Calculations

		Test 1	Test 2	Test 3	Test 4
1.	Observed pressure altitude—ft.	21,350	19,700	18,800	18,500
2.	Engine—r.p.m.	2,355	2,355	2,355	2,355
3.	Absolute manifold pressure, P_2 in. Hg	30.7	33.0	35.0	35.3
4.	Ram—in. H_2O	14.0	17.0	19.3	19.3
5.	Carburetor air temperature, T_1—°F.	19.5	23.0	25.0	30.0
6.	Free air temperature, T_a—°F.	−13.0	−4.0	+1.4	+3.0
7.	Observed b.hp.	696	753	808	810
8.	Standard air temperature, T_s—°F.	−17.1	−11.2	−8.0	−7.0
9.	C.hp. (b.hp. corrected from T_1 to T_s)	724.5	781	837	842
10.	Ram—in. Hg	1.03	1.25	1.42	1.42
11.	Pressure altitude—in. Hg	12.98	13.92	14.45	14.63
12.	Carburetor top deck pressure, P_1—in. Hg	14.01	15.17	15.87	16.05
13.	Observed pressure rise ratio—(P_2/P_1) obs.	2.19	2.18	2.21	2.20
14.	(P_2/P_1) std. (corrected from T_1 to T_s)	2.265	2.25	2.28	2.28
15.	$\frac{P_2}{(P_2/P_1) \text{ std.}}$ = (standard alt. press. for zero ram and $T_1 - T_s$ rise)	13.55	14.67	15.35	15.48
16.	Altitude (from 15)—ft.	20,350	18,430	17,330	17,120
17.	Plot c.hp. from 9 against alt. of 1 and follow constant m.a.p.-r.p.m. line to altitude from 16. See Fig. 1. Final c.hp. is: From Fig. 1 the engine critical altitude is 17,800 ft.	716	771	825	830
18.	Standard altitude pressure from 15 minus ram from 10—in. Hg	12.52	13.42	13.93	14.06
19.	Pressure altitude corresponding to 18	22,200	20,570	197	194
	Standard air temp., T_s, for 19—°F.	−20.0	−14.4	−11	−10
20.	Carburetor air temperature, T_1 for 19 from Fig. 2—°F.	17.0	19.6	...	21
21.	P_2/P_1[(P_2/P_1) std. from 15 corrected to T_1 of 20 from T_s of 19]	2.195	2.185	2.22	2.22
22.	Carburetor top deck pressure, P_1, = $\frac{P_2}{(P_2/P_1) \text{ of } 21}$	14.01	15.10	15.76	15.90
23.	P_1 from 22 minus ram from 10 = altitude pressure	12.98	13.85	14.34	14.48
24.	Altitude (from 23)—ft.	21,360	19,816	18,984	18,750
25.	Hp. at altitude of 24 (from final c.hp. of 17 along constant m.a.p.-r.p.m. line to altitude of 26), Fig. 1	725	782	838	844
26.	Standard air temperature, T_s for 26—°F.	−17.2	−11.66	−8.64	−7.9
27.	Carburetor air temperature, T_1, for 26 from Fig. 2—°F.	+18	+21	+19.4	+19.1
28.	Hp. of 25 corrected from T_s of 26 to T_1 of 27	698	762	815	820
29.	Plot hp. of 28 against altitude of 24 on Fig. 1				
30.	From Fig. 1 the airplane critical altitude is 19,200 ft.				

SAMPLE CALCULATION

A sample calculation is presented from data observed on a single-place single-engine fighter with nine-cylinder air-cooled radial engine (Table 1). The air is taken into the carburetor by a ramming scoop at the leading edge of the nose ring. The entrance to the scoop is faired to permit a minimum of turbulence at the inlet. The ram represents an increase of 17 in. H_2O pressure at the carburetor top deck as against a dynamic pressure of 25.3 in. before the entrance. Hence, the scoop effectiveness is 67 per cent of the total available pressure increase neglecting slipstream.

The increase in altitude for rated b.hp. is 2,100 ft. above that rated for the engine and 1,400 ft. above the actual engine critical altitude.

The corrected high speed of the airplane is 327.5 m.p.h. This is 7 m.p.h. in excess of what it would be at rated altitude of the engine, 3 m.p.h. of which is due to the engine exceeding its rated altitude and 4 m.p.h. due to ram on the carburetor intake.

CONCLUSION

This method of determining airplane critical altitude is not difficult to apply when the curves of effect of carburetor air temperature versus compression ratio are available. The method as used did not require special flight test equipment installed other than normal equipment for routine flight tests. It has been found possible to check several airplanes of this same type on different occasions to give the same ram effect and consistent high speeds. A later model of the airplane was quite satisfactorily checked against estimated ram from wind-tunnel tests.

FUTURE DEVELOPMENT

It is unfortunate that this problem as presented applies to an installation that is not in line with the latest developments where its application is important. The development of two-stage and exhaust turbine-driven superchargers on high-speed aircraft presents a

modification of the problem, the development of which has not yet been simplified.

In the above-mentioned installations an auxiliary stage of supercharging is involved, the corrections for which have to be made before the carburetor top deck is reached by the air charge. Beyond the carburetor top deck in the system, the problem remains essentially the same.

There is a certain pressure drop that takes place through the auxiliary stage and intercoolers in the two-stage and turbo systems which depends on the rate of flow through the system and the efficiency of the intercoolers involved.

When curves are available from which the compression ratio of the auxiliary supercharger are established and the pressure drop across the intercooler installation can be established, a method can be worked out whereby, with the aid of additional observed pressure and temperature data, corrections can be obtained which will permit determining the actual critical altitude of these installations in an airplane.

It will be desirable to standardize the temperature at the carburetor top deck to which the air through the intercoolers must be cooled in order to simplify the method. At present, different temperatures are allowed at the carburetor top deck by different agencies working on the development of the system, and assumed values of pressure loss are used for the system between the air intake and the carburetor top deck.

At best a solution of this problem will be more complicated, probably commensurate with the added complications of the supercharger installation itself. However, when more data have been established on the supercharging systems, a workable method of determining airplane critical altitude will be developed.

Erratum

In the "Letter to the Editor" by G. A. Brewer (JOURNAL OF THE AERONAUTICAL SCIENCES, August, 1942, pp. 371 and 372), Fig. 1 was lost in transit and was omitted. This figure is published herewith.

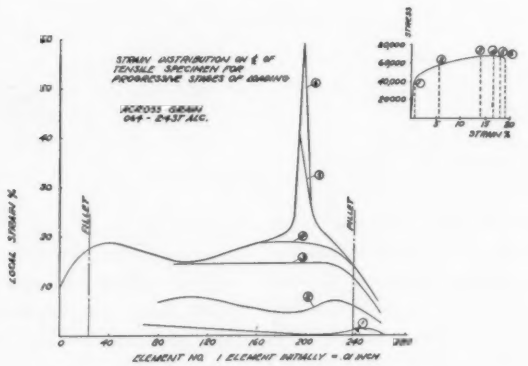

FIG. 1.

On page 371 of the August JOURNAL the illustration shown as Fig. 1 should be Fig. 2a, and on page 372 Fig. 2 should be Fig. 2b. In the second paragraph, second column, page 372, the second sentence should be changed to read: "Referring to Figs. 2a and 2b, the nonuniform nature of strain distribution along a specimen of polycrystalline material is clearly shown in the outlined zone."

Vector Solution of the Three-Degree Case of Wing Bending, Wing Torsion, Aileron Flutter

LEE ARNOLD*

Republic Aviation Corporation

Introduction

It has been seen by investigators that the two-degree analysis based on Theodorsen's[1, 2] theory is inadequate for the accurate determination of the critical flutter speeds of an oscillating airfoil-flap system. Various graphic methods of solution have been devised to eliminate the computations required in the solutions of the various two-degree cases,[3, 4] but until now no simplified solution has been developed for the three-degree case. Though the method of solution of the three-degree case is straightforward and routine in character, the actual inherent complexity of the computations involved is such that it warrants the following simplified vector method of solution.

The solution is based on the fact that the components of the vibratory determinant are complex in form (real part plus an imaginary part) and therefore can be represented by a vector in the complex plane. For a given set of physical parameters the terms of the determinant are functions of the auxiliary flutter parameter $k = \omega b/V$ and ω (ω is the flutter frequency, b the airfoil semichord, and V the flutter speed), while the remaining terms are functions only of k. Expansion of the determinant results in terms that are functions of k and ω and terms that are functions only of k. Since both of these groups are complex in form, they can still be represented by vectors.

Transposing these vectors, one on either side of the equality sign, the flutter speeds will be found by determining those values of k and ω for which the two vectors are equal.

Symbols

b = half chord of airfoil at reference station
bc = distance of flap hinge aft of mid-chord
ba = axis of rotation aft of mid-chord
ρ = mass of air per unit volume
M = mass of wing per unit length
S_α, S_β = static moments of airfoil per unit length of airfoil flap about a and flap about c
I_α, I_β = moments of inertia per unit length of airfoil flap and flap about a and c, respectively
κ = $\pi\rho b^2/M$ = the ratio of the mass of a cylinder of air of diameter equal to the chord of the airfoil to the mass of the airfoil, both taken for equal length along the span
br_α = $\sqrt{I_\alpha/M}$ = the radius of gyration
bx_α = the center of gravity distance of the airfoil from a
ω_α = the frequency of torsional vibration about a
br_β = $\sqrt{I_\beta/M}$ = reduced radius of gyration of the flap
bx_β = S_β/M = reduced center of gravity of flap from c
ω_β = frequency of torsional vibration of flap about c
ω_h = frequency of airfoil deflection
T_i = functions of c
V = critical flutter speed
ω = critical flutter frequency
k = $\omega b/V$

Mathematical Development

The equations of motion resulting from the combination of the inertia, elastic, and aerodynamic forces and moments of an oscillating airfoil-flap system, Fig. 1, at the state of steady oscillation which separates the condition of stability and instability are:

$$\left.\begin{aligned}
(\bar{R}_{a\alpha} + i\bar{I}_{a\alpha})\alpha_0 + (R_{a\beta} + iI_{a\beta})\beta_0 e^{i\varphi_1} + \\
(R_{ah} + iI_{ah})h_0 e^{i\varphi_2} = 0 \\
(R_{b\alpha} + iI_{b\alpha})\alpha_0 + (\bar{R}_{b\beta} + i\bar{I}_{b\beta})\beta_0 e^{i\varphi_1} + \\
(R_{bh} + iI_{bh})h_0 e^{i\varphi_2} = 0 \\
(R_{c\alpha} + iI_{c\alpha})\alpha_0 + (R_{c\beta} + iI_{c\beta})\beta_0 e^{i\varphi_1} + \\
(\bar{R}_{ch} + i\bar{I}_{ch})h_0 e^{i\varphi_2} = 0
\end{aligned}\right\} \quad (1)$$

where α_0, β_0, and h_0 are the maximum amplitudes of the airfoil about the torsional axis, the flap about its hinge, and the vertical displacement of the system, respectively.

Since the above equations are homogeneous, in order that solutions other than the trivial zero solution exist,

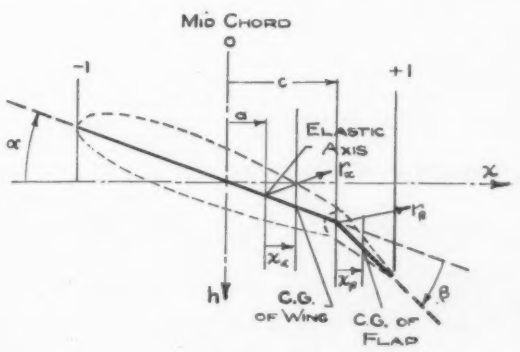

Fig. 1.

Presented at the Aerodynamics Session, Tenth Annual Meeting, I.Ae.S., New York, January 30, 1942.

* Now associated with Pratt & Whitney Aircraft Division, United Aircraft Corporation.

it is necessary that the determinant of the coefficients of Eq. (1) vanishes, so that

$$\begin{vmatrix} \bar{R}_{a\alpha} + i\bar{I}_{a\alpha} & R_{a\beta} + iI_{a\beta} & R_{ah} + iI_{ah} \\ R_{b\alpha} + iI_{b\alpha} & \bar{R}_{b\beta} + i\bar{I}_{b\beta} & R_{bh} + iI_{bh} \\ R_{c\alpha} + iI_{c\alpha} & R_{c\beta} + iI_{c\beta} & \bar{R}_{ch} + i\bar{I}_{ch} \end{vmatrix} = 0 \qquad (2)$$

The components of the determinant above are of the form

$$\left.\begin{aligned}
(\bar{R}_{a\alpha} + i\bar{I}_{a\alpha}) &= -\frac{r_\alpha^2}{\kappa} + (1 + ig_\alpha)\frac{r_\alpha^2}{\kappa}\frac{\omega_\alpha^2}{\omega^2} + R_{a\alpha}' + iI_{a\alpha} \\
(R_{a\beta} + iI_{a\beta}) &= -\frac{r_\beta^2}{\kappa} - (c-a)\frac{x_\beta}{\kappa} + R_{a\beta}' + iI_{a\beta} \\
(R_{ah} + iI_{ah}) &= -\frac{x_\alpha}{\kappa} + R_{ah}' + iI_{ah} \\
R_{b\alpha} + iI_{b\alpha} &= -\frac{r_\beta^2}{\kappa} - (c-a)\frac{x_\beta}{\kappa} + R_{b\alpha}' + iI_{b\alpha} \\
\bar{R}_{b\beta} + i\bar{I}_{b\beta} &= -\frac{r_\beta^2}{\kappa} + (1 + ig_\beta)\frac{r_\beta^2}{\kappa}\frac{\omega_\beta^2}{\omega^2} + R_{b\beta}' + iI_{b\beta} \\
R_{bh} + iI_{bh} &= -\frac{x_\beta}{\kappa} + R_{bh}' + iI_{bh} \\
R_{c\alpha} + iI_{c\alpha} &= -\frac{x_\alpha}{\kappa} + R_{c\alpha}' + iI_{c\alpha} \\
R_{c\beta} + i\bar{I}_{c\beta} &= -\frac{x_\beta}{\kappa} + R_{c\beta}' + iI_{c\beta} \\
\bar{R}_{ch} + i\bar{I}_{ch} &= -\frac{1}{\kappa} + (1 + ig_h)\frac{1}{\kappa}\frac{\omega_h^2}{\omega^2} + R_{ch}' + iI_{ch}
\end{aligned}\right\} \qquad (3)$$

where the (R_{mn}')'s and (I_{mn})'s are of the form

$$\left.\begin{aligned}
R_{a\alpha}' &= -(1/3 + a^2) + 2(1/4 - a^2)G/k - 2(1/2 + a)F/k^2 \\
R_{a\beta}' &= \frac{1}{\pi}\{T_7 + (c-a)T_1 + (T_4 + T_{10})(1/k^2) + (a + 1/2)[(T_{11}G/k) - (2T_{10}F/k^2)]\} \\
R_{ah}' &= a + 2(a + 1/2)G/k \\
R_{b\alpha}' &= \frac{1}{\pi}\{T_7 + (c-a)T_1 + T_{12}[F/k^2 - (1/2 - a)G/k]\} \\
R_{b\beta}' &= \frac{1}{\pi^2}\left[T_3 + (T_5 - T_4T_{10})1/k^2 - T_{12}\left(\frac{T_{11}}{2}G/k - T_{10}F/k^2\right)\right] \\
R_{bh}' &= 1/\pi[T_1 - T_{12}G/k] \\
R_{c\alpha}' &= a - 2(1/2 - a)G/k + 2F/k^2 \\
R_{c\beta}' &= 1/\pi[T_1 - (T_{11}G/k) + 2T_{10}F/k^2] \\
R_{ch}' &= -[1 + (2G/k)] \\
I_{a\alpha} &= -1/k\{2(a + 1/2)[(1/2 - a)F + G/k] - (1/2 - a)\} \\
I_{a\beta} &= -1/\pi k\{(a + 1/2)(T_{11}F + 2T_{10}G/k) + 2p + (1/2 - a)T_4\} \\
I_{ah} &= -2(a + 1/2)F/k \\
I_{b\alpha} &= 1/\pi k\{T_{12}[(1/2 - a)F + G/k] + p - T_1 - T_4/2\} \\
I_{b\beta} &= 1/\pi^2[(T_{11}T_{12}/2)F/k + T_{10}T_{12}G/k^2] \\
I_{bh} &= T_{12}/\pi F/k \\
I_{c\alpha} &= 1/k[2(1/2 - a)F + 2G/k + 1] \\
I_{c\beta} &= 1/\pi k[T_{11}F + (2T_{10}G/k) - T_4] \\
I_{ch} &= 2F/k
\end{aligned}\right\} \qquad (4)$$

Making the substitutions

$$\left.\begin{aligned}
\sigma_1 &= \frac{r_\alpha^2}{\kappa}\left(1 - \frac{\omega_\alpha^2}{\omega^2}\right), \quad \eta_1 = \frac{r_\beta^2}{\kappa} + (c-a)\frac{x_\beta}{\kappa} \\
\sigma_2 &= \frac{r_\beta^2}{\kappa}\left(1 - \frac{\omega_\beta^2}{\omega^2}\right), \quad \eta_2 = \frac{x_\beta}{\kappa} \\
\sigma_3 &= \frac{1}{\kappa}\left(1 - \frac{\omega_h^2}{\omega^2}\right), \quad \eta_3 = \frac{x_\alpha}{\kappa}
\end{aligned}\right\} \qquad (5)$$

into Eq. (3), there results

$$\left.\begin{aligned}
\bar{R}_{a\alpha} + i\bar{I}_{a\alpha} &= -\sigma_1 - ig_\alpha\left(\sigma_1 - \frac{r_\alpha^2}{\kappa}\right) + (R_{a\alpha}' + iI_{a\alpha}) \\
\bar{R}_{b\beta} + i\bar{I}_{b\beta} &= -\sigma_2 - ig_\beta\left(\sigma_2 - \frac{r_\beta^2}{\kappa}\right) + (R_{b\beta}' + iI_{b\beta}) \\
\bar{R}_{ch} + i\bar{I}_{ch} &= -\sigma_3 - ig_h\left(\sigma_3 - \frac{1}{\kappa}\right) + (R_{ch}' + iI_{ch}) \\
R_{a\beta} + iI_{a\beta} &= -\eta_1 + (R_{a\beta}' + iI_{a\beta}) \\
R_{b\alpha} + iI_{b\alpha} &= -\eta_1 + (R_{b\alpha}' + iI_{b\alpha}) \\
R_{bh} + iI_{bh} &= -\eta_2 + (R_{bh}' + iI_{bh}) \\
R_{c\beta} + iI_{c\beta} &= -\eta_2 + (R_{c\beta}' + iI_{c\beta}) \\
R_{ah} + iI_{ah} &= -\eta_3 + (R_{ah}' + iI_{ah}) \\
R_{c\alpha} + iI_{c\alpha} &= -\eta_3 + (R_{c\alpha}' + iI_{c\alpha})
\end{aligned}\right\} \qquad (6)$$

For fixed values of c and a, the above R_{mn}' and I_{mn} terms are functions only of k, so that each term $R_{mn} + iI_{mn}$ is made up of a term containing the inertia, elastic and friction effects, and a term $R_{mn}' + iI_{mn}$ dependent only upon the auxiliary flutter parameter, k.

Since each term of Eq. (6) is complex in form, it can be represented by a vector in the complex R_{mn}, I_{mn} plane. These vectors will be of magnitude A_{mn} and will form the angle ψ_{mn} with the R_{mn} axis.

Each of these vectors will take the form

$$R_{mn} + iI_{mn} = A_{mn}e^{i\psi_{mn}}$$

and

$$\bar{R}_{mn} + i\bar{I}_{mn} = \bar{A}_{mn}e^{i\bar{\psi}_{mn}} \qquad (7)$$

Substituting Eq. (7) in Eq. (2), expanding, and then placing all barred terms on the right-hand side and unbarred on the left, there results

$$\begin{aligned}
&A_{a\beta}A_{bh}A_{c\alpha}e^{i(\psi_{a\beta}+\psi_{bh}+\psi_{c\alpha})} + A_{b\alpha}A_{c\beta}A_{ah}e^{i(\psi_{b\alpha}+\psi_{c\beta}+\psi_{ah})} = \\
&\bar{A}_{a\alpha}A_{bh}A_{c\beta}e^{i(\bar{\psi}_{a\alpha}+\psi_{bh}+\psi_{c\beta})} + \bar{A}_{b\beta}A_{ah}A_{c\alpha}e^{i(\bar{\psi}_{b\beta}+\psi_{ah}+\psi_{c\alpha})} + \\
&\bar{A}_{ch}A_{a\beta}A_{b\alpha}e^{i(\bar{\psi}_{ch}+\psi_{a\beta}+\psi_{b\alpha})} + \bar{A}_{a\alpha}\bar{A}_{b\beta}\bar{A}_{ch}e^{i(\bar{\psi}_{a\alpha}+\bar{\psi}_{b\beta}+\bar{\psi}_{ch})}
\end{aligned}$$

This has the form

$$H_1e^{i\theta_1} + H_2e^{i\theta_2} = \bar{H}_3e^{i\bar{\theta}_3} + \bar{H}_4e^{i\bar{\theta}_4} + \bar{H}_5e^{i\bar{\theta}_5} + \bar{H}_6e^{i\bar{\theta}_6}$$

or

$$He^{i\theta} = \bar{H}e^{i\bar{\theta}} \qquad (8)$$

Construction and Use of Vector Curves

Since the procedures for the construction of each of the vector plots $\bar{R}_{mn} + i\bar{I}_{mn}$ are similar, only the plot of $\bar{R}_{a\alpha} + i\bar{I}_{a\alpha}$ will be explained completely. It is recalled that

$$\bar{R}_{a\alpha} + i\bar{I}_{a\alpha} = -\sigma_1 - ig_a\left(\sigma_1 - \frac{r_a^2}{\kappa}\right) + (R_{a\alpha}' + iI_{a\alpha})$$

Since the expression $R_{a\alpha}' + iI_{a\alpha}$ is purely a function of k for a fixed c and a, it can be plotted independently of the physical parameters as shown in Fig. 2.

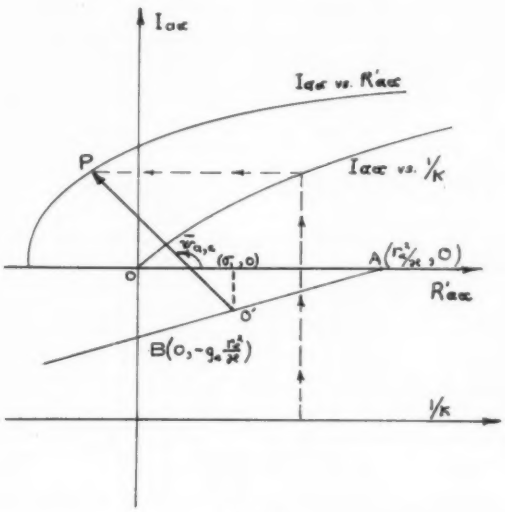

Fig. 2.

The curves $I_{a\alpha}$ vs. $R_{a\alpha}'$ and $I_{a\alpha}$ vs. $1/k$ are plotted for permanent use. (These curves have been plotted for $a = -0.1, -0.2, -0.3, -0.4, -0.5$.) A straight line is drawn through the points, A measured a positive distance r_α^2/κ on the real axis, and B measured a distance $-g_\alpha r_\alpha^2/\kappa$ on the imaginary axis. A point is dropped from $R_{a\alpha}' = \sigma_1$ in a direction perpendicular to the $R_{a\alpha}'$ axis to the line $\overline{AB}$ to form the origin, 0, of the vector. Then from the chosen value of $1/k$ on the $1/k$ axis a point is determined on the $I_{a\alpha}$ vs. $R_{a\alpha}'$ curve which when transmitted parallel to the $R_{a\alpha}'$ axis will determine the point P, the end point of the vector, on the $I_{a\alpha}$ vs. $R_{a\alpha}'$ curve.

Identical procedure was followed for the determination of the vector

$$\bar{R}_{b\beta} + i\bar{I}_{b\beta} = -\sigma_2 - ig_\beta(\sigma_2 - r_\beta^2/\kappa) + (R_{b\beta}' + iI_{b\beta})$$

The point A will be at $(r_\beta^2/\kappa, 0)$, the point B at $(0, -g_\beta r_\beta^2/\kappa)$, and σ_2 will be used instead of σ_1.

Also for the determination of the vector

$$\bar{R}_{ch} + i\bar{I}_{ch} = -\sigma_3 - ig_h[\sigma_3 - (1/\kappa)] + (R_{ch}' + iI_{ch})$$

The point A will be at $(1/\kappa, 0)$, the point B at $(0, -g_h(1/\kappa))$, and σ_3 will be used instead of σ_1. σ_1, σ_2 and σ_3 have a definite relation to each other and cannot be chosen at random.

For a given value of σ_1 the corresponding σ_2 and σ_3 are determined from the system shown in Fig. 3.

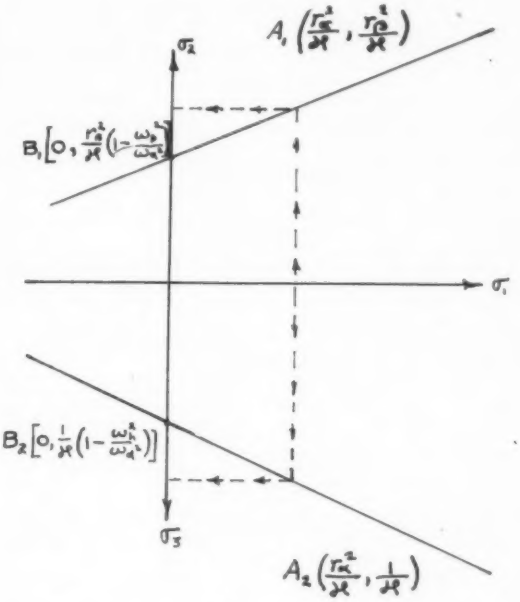

Fig. 3

For the unbarred terms

$$R_{mn} + iI_{mn} = -\eta_t + (R_{mn}' + iI_{mn})$$

$R_{mn}' + iI_{mn}$ has been plotted for a complete range of k's for various c and a combinations. The procedure is similar to that employed in determining the barred vectors except that the vector origin is located at the point $R_{mn}' = \eta_t$.

Procedure

1. The lengths A_{mn} and the angles ψ_{mn} are measured and tabulated for a few values of k in a practical range.
2. The lengths $\bar{A}_{mn}$ and the angles $\bar{\psi}_{mn}$ are measured for a range of σ_1's (and the corresponding σ_2's and σ_3's) and a range of k's to be used with each value of σ_1.
3. The values of A_{mn}, ψ_{mn} are substituted into the unbarred terms of the left side of Eq. (8) forming the vector $He^{i\theta}$, and then the values A_{mn}, ψ_{mn}, $\bar{A}_{mn}$ and $\bar{\psi}_{mn}$ are substituted into the right-hand side of Eq. (8) forming the various vectors $\bar{H}e^{i\bar{\theta}}$.
4. Plot H vs. θ for each value of k, and H vs. k as shown in Fig. 4.
5. Plot $\bar{H}$ vs. $\bar{\theta}$ for a fixed $k = \bar{k}$ and varying σ_1's, and $\bar{\theta}$ vs. σ_1.
6. Superimpose the H, θ curve onto the $\bar{H}$, $\bar{\theta}$ curve.
7. Translate P_1, P_2, P_3, ..., P_n horizontally to the H vs. k curve and then down to the ordinate $\bar{k}_1$, $\bar{k}_2$, ..., $\bar{k}_n$, respectively, in the k, $\bar{k}$ plane. These $(k, \bar{k})$ points

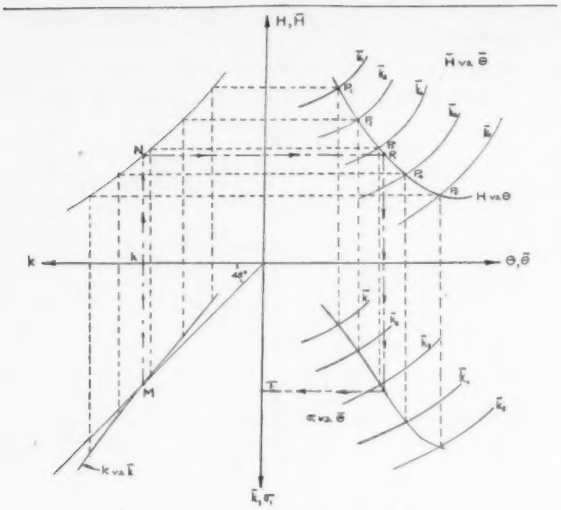

FIG. 4.

will be the loci of a curve in the k, $\bar{k}$ plane. Where the bisector of the k and $\bar{k}$ axes intersects the k, $\bar{k}$ curve, the point M is determined.

8. Translate P_1, P_2, ..., P_n vertically downward to the $\bar{k}$ curves of the σ_1 vs. $\bar{\theta}$ group. These points on $\bar{k}_1$, $\bar{k}_2$, ..., $\bar{k}_n$ will form the locus of a (k, σ_1) curve.

9. Translate M vertically upward to the point N on the H vs. k curve, then from N horizontally to R on the H vs. θ curve, then down vertically to S on the k vs. σ_1 curve, and finally horizontally to T on the σ_1 axis.

10. Where $\overrightarrow{MN}$ intersects the k axis k is determined, and the point T determines σ_1.

11. From the relations $\sigma_1 = (r_\alpha^2/\kappa)[1 - (\omega_\alpha^2/\omega^2)]$ and $k = \omega b/V$, there results

$$V = \frac{\omega_\alpha b}{k} \frac{1}{\sqrt{1 - [\sigma_1/(r_\alpha^2/\kappa)]}} \tag{9}$$

from which the flutter speeds are determined.

REFERENCES

[1] Theodorsen, Theodore, *General Theory of Aerodynamic Instability and the Mechanism of Flutter*, N.A.C.A. T.R. No. 496, 1934.

[2] Theodorsen, Theodore, and Garrick, I. E., *Mechanism of Flutter: A Theoretical and Experimental Investigation of the Flutter Problem*, N.A.C.A. T.R. No. 685, 1940.

[3] Kassner, R., and Fingado, H., *Das Ebene Problem der Flugelschwingung*, Luftfahrtforschung, Vol. 13, No. 11, pp. 374–390, November 20, 1936.

[4] Bergen, W. B., and Arnold, L., *Graphical Solution of the Bending Aileron Case of Flutter*, Journal of the Aeronautical Sciences, Vol. 7, No. 12, pp. 495–508, October, 1940.

Predicting Stiffener and Stiffened Panel Crippling Stresses

HAROLD B. CROCKETT*
Lockheed Aircraft Corporation

SUMMARY

An empirical method is presented for predicting the crippling stress at $L/\rho \leqslant 20$ of 24S-T Alclad bent-up sheet stiffeners, 24S-RT Alclad bent-up sheet stiffeners, and 24S-T extruded stiffeners acting alone or in conjunction with 24S-T Alclad sheet as a panel. It is also shown that predicted column curves may be constructed by drawing a straight line tangent to the Euler column curve ($c = 1.5$) through the predicted crippling stress at $L/\rho = 20$ (except through $L/\rho = 40$ for *extrusion* stiffened *panels*); the predicted stress at $L/\rho = 20$ (or 40) locates the horizontal cutoff for the section of the column curve with $L/\rho \leqslant 20$ (or 40).

The general method, which consists of summing the crippling loads of the component elements of the stiffener and then dividing by the summation of the elemental areas to obtain the crippling stress, is discussed in several texts on airplane structural analysis; however, enough test data have not been available heretofore to establish general empirical curves for predicting the strength of any stiffener or stiffened panel of reasonable proportions.

INTRODUCTION

AIRPLANE STRUCTURAL ENGINEERS continually are faced with the problem of finding the crippling (*local* compressive failure) strength of aluminum alloy stiffeners and stiffened panels. If test results are not available, the engineer ordinarily estimates the total load the stiffener will carry by applying theoretic equations (such as those in references 1 and 2) to determine the buckling loads of the various flat and curved elements of the stiffener and then summing the loads carried by the elements. This paper gives an empirical method for predicting the crippling stress of stiffeners and stiffened panels by using design curves that are trial-and-error variations from the theoretic to give the best possible agreement with test data.

It is suggested that one read this paper entirely through before attempting to use the curves and tables given in the first part. Especially should all limitations of L/ρ, b/t, etc., be studied, as well as the notes appended to Table 1. Worth-while emphasis may be placed on the fact that Table 1 is a compact device for showing cross-section sketches *to scale* of all the specimens offered as the basis for this report, besides demonstrating typical examples of stiffeners to which are applicable the "stability shape factors." These factors are general empirical coefficients indicating the relative strength of *any* (1) vertical-legged and (2) slanting-legged stiffeners *judged by the reader* to lie within the range of the curves given.

Many engineers will not care to extrapolate the design curves of Figs. 2 and 3 nearly as far as shown; however, in this respect, the following preliminary statements may be of assistance:

1. The extrapolated portions of the design curves for the flat elements of stiffeners (Fig. 2) fair into the

TABLE 1. STABILITY SHAPE FACTORS

$F_{cc} = K F_{cc1}$

STIFFENERS *	K **
24 ST ALCLAD STIFFENERS, 24 ST ALCLAD SHEET	
VERTICAL LEGS: LS 160, 161, 166; XLS 165; X-785-A, X-785-B; X-785-D; LS 140	1.07
SLANTING LEGS: $t_{sh} < t_{st}$ BY 1 GAGE; LS 173; LS 174; X-785-C	1.00
24 SRT ALCLAD STIFFENERS, 24 ST ALCLAD SHEET	
VERTICAL LEGS: LS 160, LS 161, XLS 165, X-785-A, X-785-B, X-785-D + LS 160 MOD; LS 156; LS 157	1.08
SLANTING LEGS: LS 174, X-785-C + ℄ SYM.; LS 152; LS 153; LS 154	.92
24 ST EXTRUDED SHAPES, 24 ST ALCLAD SHEET	
BULB ANGLES AND TEES: DOUBLE; LS 222, 220; LS 223, 224; LS 247, 248, 249; LS 234	1.08
ANGLES, TEES, AND CHANNELS: LS 219, 208; LS 209, 200, 210; LS 236, 232; LS 264	1.00

NOTES:

*(a) The stiffeners shown are those tested. K applies to any stiffeners judged to lie within the range of the method given. (b) One division represents $1/4$ in. (c) The underlined identification numbers indicate that those stiffeners were tested with, and in some cases also without, sheet attached.

** K is given for stiffeners of various materials and angularity of legs assuming that thickness of sheet is less than, or equal to, thickness of stiffener unless otherwise indicated.

Received May 13, 1942.

* Stress Engineer.

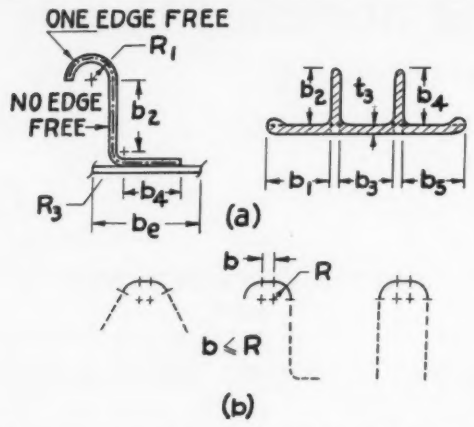

FIG. 1. Conventions. (a) Sheet and extruded stiffener conventions. The convention for determining the areas of elements of extruded stiffeners is to be used in connection with predicting the average crippling stress; the load carried by the stiffener is the product of the average stress and the total area of the stiffener. (b) Sketch for special rule given.

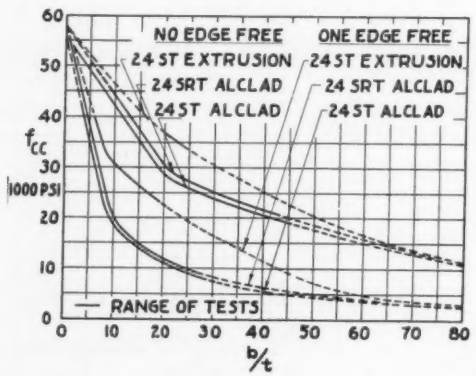

FIG. 2. Crippling stress of flat elements of 24S stiffeners in compression.

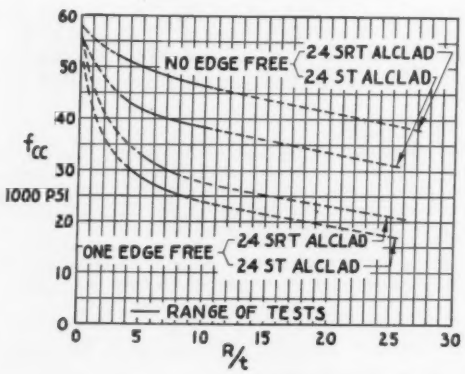

FIG. 3. Crippling stress of circular elements of 24S Alclad sheet stiffeners in compression.

classic theoretic buckling curves as b/t approaches 80. Results of Lockheed tests detailed by Fischel[3] show that theoretic curves giving the strength in compression of panels assumed simply supported (no edge free) are increasingly conservative for $b/t > 45$ and that at b/t of 100 these stiffened panels act as would theoretically fixed-edge panels. Flat elements of stiffeners act similarly.

2. The extrapolated portions of the design curves for the no-edge-free curved elements of stiffeners (Fig. 3) lie completely within the range of, and indicate compressive strength values only a little greater than, those curves for circular corrugations given in Fig. 5-4 of reference 1. In fact, good agreement exists between the column stress at $L/\rho = 20$ given by Fig. 5-4 of reference 1 for circular corrugations and the crippling stress computed using the present design curves and the logical assumption that one-half pitch-width of a circular corrugation acts as two circular quadrants on either side of a flat element two quadrants wide (all three elements assumed to have two sides simply supported, i.e., with no edge free).

3. The second part of the paper contains the complete test results upon which the curves of Figs. 2 and 3 are based. The quantity of data presented should instill the engineer with confidence in the design curves and afford him the opportunity to correlate his own private method for predicting stiffener strengths with these tests.

PREDICTING CRIPPLING STRESSES: $L/\rho \leqslant 20$

General Method

The crippling stress of a stiffener may be predicted by summing the crippling loads of the component elements of the stiffener and then dividing by the summation of the elemental areas, as expressed by Eq. (1):

$$F_{cc} = K \frac{\Sigma\, b_n t_n f_{cn}}{\Sigma\, b_n t_n} = K F_{cc1} \qquad (1)$$

where

F_{cc} = final predicted crippling stress, lbs. per sq.in., for $L/\rho \leqslant 20$
F_{cc1} = uncorrected predicted stress = $\Sigma\, b_n t_n f_{cn} / \Sigma\, b_n t_n$
K = the stability shape factor given in Table 1
$b_n t_n$ = area of individual element, sq.in.
f_{cn} = average ultimate stress of the individual element, given empirically by Figs. 2 and 3 for flat and curved elements, respectively, lbs. per sq.in.
ρ = the radius of gyration of the stiffener alone about an axis parallel to the sheet in a stiffener-sheet combination, in.
L = length of stiffener or panel, in.

The crippling stress of a stiffened panel may be determined as above by considering the effective width of sheet acting with the stiffener to be a simply supported —that is, no-edge-free—element of the stiffener. The reader will recall that by definition the effective width

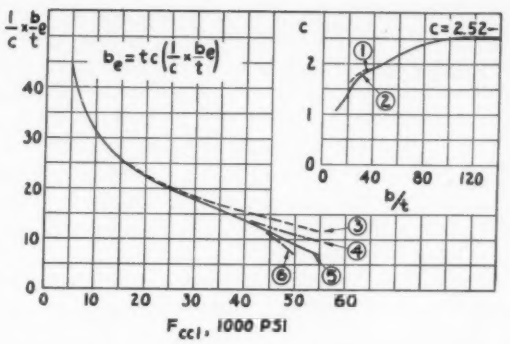

FIG. 4. Effective widths at various stiffener stresses of 24S Alclad sheet in compression. *Key:* (1) 24S-RT Alclad sheet; (2) 24S-T Alclad sheet; (3) 24S-RT Alclad sheet and stiffeners; (4) 24S-T Alclad sheet, 24S-RT Alclad stiffeners; (5) 24S-T Alclad sheet and stiffeners; (6) 24S-T Alclad sheet, 24S-T extruded stiffeners.

of sheet is said to act at the average stiffener stress. This is the basis upon which the effective width is estimated from Fig. 4. However, to predict the panel crippling stress *the effective width is then assumed to be a no-edge-free element of the stiffener-sheet combination* and to act at the much lower than average stress thereof. The procedure is discussed fully in another section.

The conventions adopted for measuring b, b_e, t, and R are shown in Fig. 1a, where

b = developed width of element, in.
b_{sh} = stiffener spacing (width sheet), in.
b_e = effective width of sheet acting with stiffener, in.; estimated from Fig. 4
t_{st} = thickness of stiffener, in.
t_{sh} = thickness of sheet, in.
R = the centerline radius of a curved element, in.

Fig. 1a also indicates clearly the significance of the terms "one-edge-free" (one edge simply supported) and "no-edge-free" (two edges simply supported) stiffener elements.

An arbitrary rule is stated as follows to take care of instances when a narrow flat element lies between two curved elements: If two curved elements of equal radius (centers on same side of sheet) are separated as shown in Fig. 1b by a flat element with width $b \leqslant R$, the average stress of the three elements is taken as that of a curved element of radius $R' = R + (b/2)$.

Predicting Crippling Stress of Stiffener Acting Alone

It is desirable first to give a detailed example of predicting the crippling stress of a stiffener acting alone and then to consider a stiffener with sheet attached, because the techniques are slightly different.

An outline of the steps involved in predicting the strength of a stiffener acting alone follows:

(1) Make a table as shown in Fig. 5. (a) Enter sketch, b, nominal R, actual R/t, b/t. (b) Obtain f_{cn} from Figs. 2 and 3. (c) Enter $b_n t_n$, $b_n t_n f_{cn}$, $\Sigma\, b_n t_n$, and $\Sigma\, b_n t_n f_{cn}$. (d) Compute $F_{ccl} = \Sigma\, b_n t_n f_{cn} / \Sigma\, b_n t_n$.

(2) Find the stability shape factor in Table 1 and compute $F_{cc} = KF_{ccl}$.

Example 1: Given 0.040 gauge LS 160 24S-T Alclad section. Find the crippling stress of a column with $L/\rho = 20$.

(1) Make a table as shown in Fig. 5.

$$F_{ccl} = \frac{\Sigma\, b_n t_n f_{cn}}{\Sigma\, b_n t_n} = \frac{2{,}311}{0.0807} = 28{,}600 \text{ lbs. per sq.in.}$$

From Table 1, for a vertical-legged 24S-T Alclad stiffener, $K = 1.07$.

(2) Therefore, the crippling stress

$$F_{cc} = KF_{ccl} = 1.07 \times 28{,}600 = 30{,}600 \text{ lbs. per sq.in.}$$

For this stiffener the corrected test crippling stress $F_{cc}' = 32{,}400$ lbs per sq.in. (see Table 2), or the test stress is 6.0 per cent of the predicted stress higher than the predicted stress.

Predicting Crippling Stress of Stiffener Acting with Sheet

Ordinarily the addition of sheet to a stiffener in compression reduces the crippling stress of the stiffener because, as the sheet buckles, wrinkles tend to form across the stiffeners, even though prevented from actually doing so by proper rivet or spot-weld spacing. This tendency causes a side load on the stiffener which reduces the crippling stress. By assuming that the effective width of sheet acting with the stiffener becomes a no-edge-free element in the stiffener-sheet combination, it is possible to estimate the crippling stress of the combination. The effective width to use as a no-edge-free element may be determined approximately from Fig. 4, the development of which is discussed by Fischel,[3] by assuming the stress of the combination to be F_{ccl} of the stiffener alone. The latter assumption is accurate

1	2	3	4	5	6	7	8	9	10	11
Sketch	Part No. n	t_n	b_n	b_n/t_n	R' Nominal	R/t Actual	f_{cn}	$b_n t_n$	$b_n t_n f_{cn}$	F_{ccl}
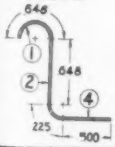	1	0.040	0.646		3/16	5.2	28,200	0.0258	729	
	2	0.040	0.648	16.2			33,700	0.0259	874	
	3	0.040	0.225		1/8	3.6	43,600	0.0090	392	
	4	0.040	0.500	12.5			15,800	0.0200	316	
								0.0807	2,311	28,600

FIG. 5.

TABLE 2

24S-T Alclad Stiffeners, 24S-T Alclad Sheet

1	2	3	4	5	6	7	8
Stiffener*	Stiffener Gauge, t_{st}	Sheet† Gauge, t_{sh}	F_{cc}', Lbs. per Sq.in., Test Corrected	F_{ccl}, Lbs. per Sq.in.	K	Predicted $F_{cc} = KF_{ccl}$, Lbs. per Sq.in.	Margin, $\left(\frac{F_{cc}'}{F_{cc}} - 1\right)100$
LS 160	0.025		23,700	21,400	1.07	22,500	5.3
	0.032	0.020	28,300	24,100	1.07	25,800	9.7
	0.032	0.025	27,500	23,400	1.07	25,000	10.0
	0.032	0.032	25,800	22,400	1.07	24,000	7.5
	0.032	0.040	23,500	21,300	1.07	22,800	3.1
	0.040		32,400	28,600	1.07	30,600	6.0
	0.040	0.020	30,300	26,400	1.07	28,200	7.4
	0.040	0.025	28,900	26,100	1.07	27,900	3.7
	0.040	0.032	27,500	24,400	1.07	26,100	5.4
	0.051	0.020	36,500	30,200	1.07	32,300	13.0
	0.051	0.025	34,500	29,600	1.07	31,700	8.8
	0.051	0.032	32,200	28,400	1.07	30,400	6.0
	0.051	0.040	33,100	27,100	1.07	29,000	14.1
	0.064		43,300	35,000	1.07	37,400	15.8
	0.064	0.025	37,300	32,800	1.07	35,100	6.3
	0.064	0.032	32,300	31,600	1.07	33,800	− 4.4
	0.064	0.040	32,600	30,400	1.07	32,500	0.3
	0.081		45,300	38,400	1.07	41,100	10.2
$W = 1/8$ as above	0.032	0.040	24,050	21,300	1.07	22,800	5.5
$W = 3/4$	0.032	0.040	22,000	19,700	1.07	21,100	4.3
$W = 1$	0.032	0.040	17,400	19,100	1.07	20,400	−14.7‡
LS 161	0.025		21,500	20,400	1.07	21,800	− 1.4
	0.040		29,300	26,900	1.07	28,800	1.8
	0.064		41,600	34,500	1.07	36,900	12.7
	0.081		45,500	38,200	1.07	40,900	11.2
LS 166	0.051	0.032	35,500	32,100	1.07	34,400	3.2
XLS 165	0.025		20,700	19,100	1.07	20,400	1.5
	0.040		26,600	25,100	1.07	26,800	− 0.8
X-785-A	0.025		19,600	17,200	1.07	18,300	7.1
	0.040		27,000	25,400	1.07	27,200	− 0.7
	0.064		41,100	36,800	1.07	39,400	4.3
	0.081		46,000	42,000	1.07	45,000	2.2
X-785-B	0.025		18,400	15,600	1.07	16,700	10.2
	0.040		25,600	23,200	1.07	24,800	3.2
	0.064		34,900	32,600	1.07	34,900	0
	0.081		44,200	38,700	1.07	41,400	6.8
X-785-C	0.025		19,600	17,500	1.00	17,500	12.0
	0.040		26,200	26,200	1.00	26,200	0
	0.064		37,700	37,400	1.00	37,400	0.8
	0.081		45,200	41,200	1.00	41,200	9.7
X-785-D	0.025		22,000	20,500	1.07	21,900	0.5
	0.040		31,100	29,100	1.07	31,100	0
	0.064		42,900	39,600	1.07	42,400	1.2
	0.081		47,500	42,400	1.07	45,400	4.6
LS 140	0.040		29,000	27,400	1.07	29,300	− 1.0
LS 173	0.032	0.025	26,500	25,600	1.00	25,600	3.5
	0.032	0.032	26,100	24,300	1.00	24,300	7.4
LS 174	0.032	0.025	27,400	26,400	1.00	26,400	3.8
	0.040	0.040	19,600	25,200	1.00	25,200	−22.2**
	0.051	0.032	32,400	28,500	1.00	28,500	13.7
	0.051	0.040	32,400	27,900	1.00	27,900	16.1
	0.064	0.032	37,100	31,900	1.00	31,900	16.3

* Sketches shown drawn to scale in Table 1.

† No sheet gauge given indicates stiffener tested alone.

‡ Stiffener of poor proportions.

** Limiting thickness in Table 1 based on this point. Test might be bad, although three points on column curve agree well.

enough considering the empirical nature of the method. Since b_e/t_{sh} ordinarily is about 40, the stress of the effective element is low. As a result, the predicted average crippling stress of the stiffener-sheet combination is lower than that of the stiffener acting alone.

An outline of the steps involved in predicting the strength of a stiffener acting with sheet follows:

(1) Estimate F_{ccl} of the stiffener alone as detailed above.

(2) Knowing the dimensions of the panel, use Fig. 4 to find the effective width of sheet b_e acting with the stiffener at the stress F_{ccl}.

(3) Calculate b_e/t_{sh} and determine f_{cn} for the no-edge-free effective sheet element.

(4) Calculate $b_n t_n$ and $b_n t_n f_{cn}$ for the effective sheet element; add these to the $\Sigma\, b_n t_n$ and $\Sigma\, b_n t_n f_{cn}$, respectively, obtained in step 1 (table similar to that of Fig. 5).

(5) Compute F_{ccl} of the combination

$$\text{New } F_{ccl} = \Sigma\, b_n t_n f_{cn} / \Sigma\, b_n t_n$$

(6) Find the stability shape factor in Table 1 and compute $F_{cc} = KF_{ccl}$.

Example 2: Given the 0.040 gauge LS 160 24S-T Alclad section of Example 1 acting with 0.025 gauge 24S-T Alclad sheet in a panel having $b_{sh}/t_{sh} = 94$ and $L/\rho = 20$. Find the crippling stress of the stiffener, effective-sheet combination.

(1) From Example 1, $F_{ccl} = 28{,}600$, $\Sigma\, b_n t_n = 0.0807$ and $\Sigma\, b_n t_n f_{cn} = 2{,}311$.

(2) From Fig. 4, for $b_{sh}/t_{sh} = 94$, $c = 2.47$. From Fig. 4, for $F_{ccl} = 28{,}600$ lbs. per sq.in., $(1/c)(b_e/t_{sh}) = 18.4$. Therefore, $b_e = (1/c)(b_e/t_{sh})ct_{sh} = (18.4)(2.47) \times (0.025) = 1.135$ in., and $b_e/t_{sh} = 1.135/0.025 = 45.5$. From Fig. 2, for $b_e/t_{sh} = 45.5$, $f_{cn} = 18{,}900$ lbs. per sq.in.

(3)	$\Sigma\, b_n t_n$	$= 0.0807$
	$(1.135)(0.025)$	$= 0.0284$
	New $\Sigma\, b_n t_n$	$= 0.1091$
	$\Sigma\, b_n t_n f_n$	$= 2{,}311$
	$(1.135)(0.025)(18{,}900)$	$= 536$
	New $\Sigma\, b_n t_n f_n$	$= 2{,}847$

New $F_{ccl} = 2{,}847/0.1091 = 26{,}100$ lbs. per sq.in.

(4) From Table 1, for a 24S-T Alclad stiffener with vertical legs, $K = 1.07$.

$$F_{cc} = KF_{ccl} = (1.07)(26{,}100) = 27{,}900 \text{ lbs. per sq.in.}$$

(5) For this stiffener the corrected test crippling stress $F_{cc}' = 28{,}900$ lbs. per sq.in. (see Table 2), or the test stress is 3.7 per cent higher than the predicted stress.

Stiffener Column Curves

After the crippling stress of a stiffener or stiffener-sheet combination has been determined, that stress may be used as the cutoff for an approximate column curve constructed in the following manner:

(1) Make a graph with stress as ordinate and L/ρ as abscissa.

(2) For $L/\rho \leqslant 20$, make stress equal to F_{cc} of the stiffener or combination (except for $L/\rho \leqslant 40$ for 24S-T extrusion stiffened panels).

(3) Construct Euler column curve

$$F_c = c\pi^2 E/(L/\rho)^2$$

where

c = 1.5 for design
L = length of column, in.
E = modulus of elasticity, lbs. per sq.in.
ρ = radius of gyration of stiffener alone, in.

(4) Draw a straight line tangent to the Euler curve through the crippling stress cutoff point at $L/\rho = 20$ (but at $L/\rho = 40$ for 24S-T extrusion stiffened panels).

Fig. 6 shows a comparison between the predicted column curve and the corrected test curve for LS161—0.064 24S-RT Alclad stiffeners on 0.040 24S-T Alclad sheet.

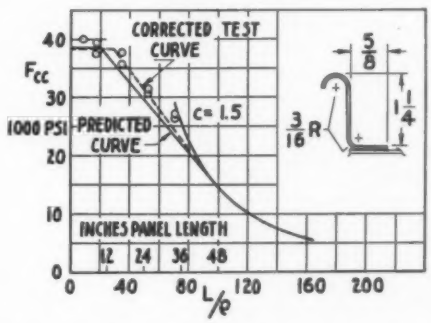

FIG. 6. Column curve: LS 161–0.064 24S-RT Alclad stiffener on 0.040 24S-T Alclad sheet. $A = 0.150$ sq. in. $\rho = 0.481$ in.

SUMMARY OF TEST RESULTS

Tables 2, 3, and 4 give a summary of the various stiffeners and panels tested as well as a comparison of the test and predicted crippling stresses. For L/ρ approximately equal to 20 there were 137 different stiffener and stiffener-sheet combinations tested. All of the specimens were tested in duplicate or triplicate. Also tests (in duplicate) were made at other L/ρ values (from one to three additional points) for the panels in order to determine column curves. All of the specimens were tested flat-ended, which accounts for some of the scatter. In accordance with general practice, the compressive stresses were corrected to minimum guaranteed properties using the procedure given in the ANC-5 Sec. 1.543; and the test column curves, having an end fixity constant $c = 3$, were corrected to the design value of $c = 1.5$. The tests show the fixity value of $c = 1.5$ particularly to be applicable in the design of wing and fuselage compression panels.

The dimensions of the stiffeners are shown in Table 1.

TABLE 3

24S-RT Alclad Stiffeners, 24S-T Alclad Sheet

1	2	3	4	5	6	7	8
Stiffener*	Stiffener Gauge, t_{st}	Sheet† Gauge, t_{sh}	F_{cc}', Lbs. per Sq.in., Test Corrected	F_{ccl}, Lbs. per Sq.in.	K	Predicted $F_{cc} = KF_{ccl}$, Lbs. per Sq.in.	Margin, $\left(\frac{F_{cc}'}{F_{cc}} - 1\right)100$
LS 160	0.025		25,900	24,100	1.08	26,000	− 0.4
	0.032	0.020	32,500	25,300	1.08	27,300	19.0
	0.032	0.025	28,000	24,400	1.08	26,400	6.1
	0.032	0.032	30,200	24,100	1.08	26,000	16.2
	0.040		35,900	31,800	1.08	34,400	4.4
	0.040	0.020	35,200	29,700	1.08	32,100	9.7
	0.040	0.025	35,100	29,000	1.08	31,400	11.8
	0.040	0.032	30,300	28,000	1.08	30,200	0.3
	0.051	0.020	41,500	33,700	1.08	36,400	14.0
	0.051	0.025	39,800	33,200	1.08	35,800	11.2
	0.051	0.032	38,700	31,500	1.08	33,500	15.5
	0.051	0.040	34,400	30,000	1.08	32,400	6.2
	0.051	0.051	34,000	28,300	1.08	30,600	11.1
LS 160 Modified	0.032	0.032	37,800	35,500	1.08	38,400	− 1.6
	0.032	0.032	38,500	31,200	1.08	33,700	14.2
LS 161	0.025		23,200	22,800	1.08	24,600	− 5.7
	0.032	0.040	23,200	22,800	1.08	24,600	− 5.7
	0.040		30,400	29,600	1.08	32,000	− 5.0
	0.040	0.040	28,600	25,400	1.08	27,400	4.4
	0.051	0.025	38,200	32,000	1.08	34,600	10.4
	0.051	0.040	35,600	29,600	1.08	32,000	11.2
	0.051	0.051	32,000	28,000	1.08	30,200	6.0
	0.051	0.064	34,000	26,500	1.08	28,600	18.9
	0.064		49,500	39,600	1.08	42,800	15.7
	0.064	0.040	38,700	36,000	1.08	38,900	− 0.5
X-LS 165	0.025		25,600	21,700	1.08	23,400	9.4
	0.040		34,700	27,600	1.08	29,800	16.4
	0.025	0.025	27,600	27,000	1.08	29,200	− 5.5
	0.040	0.025	33,500	33,500	1.08	36,200	− 7.5
	0.064	0.025	41,000	35,000	1.08	37,800	8.5
X-785-A	0.025		22,400	19,500	1.08	21,000	6.7
	0.040		31,100	28,000	1.08	30,200	3.0
	0.064		48,500	41,000	1.08	44,300	9.5

* Sketches shown drawn to scale in Table 1. † No sheet gauge given indicates stiffener tested alone.

The panels tested had two or three stiffeners, with stiffener spacings of 4, 5, or 6 in. in most cases. Many of the stiffeners were riveted to the sheet with 1-in. spacing, although some were spot-welded. In some instances of V-stiffeners (greatest use of spot welds) the spots were prestressed as a result of small waves left in the stiffener by the forming brake; these waves were noticeable only in the heavier gauge sheets. In connection with possible evaluation of scatter, it is well to note that no definite measurements were made of maximum crookedness (initial lateral deflection) to length ratio, a factor which the Aluminum Company research engineers[4] try to hold to less than 1 part in 3,000 for stiffeners tested alone.

DISCUSSION

It is not the purpose of this discussion to go into any long explanations of the reasons for the scatter of individual test points but rather to make a few itemized comments concerning (1) the validity of the test results as a whole and (2) the use of the summary of results in conjunction with the curves for predicting crippling stress as an aid in designing stiffened panels.

Validity of Prediction Curves and Test Results

Fig. 7 is a statistical presentation of the percentage margins of test over predicted stress tabulated in Column 8 of Tables 2, 3, and 4. Fig. 7 shows frequency curves for the various stiffener materials—

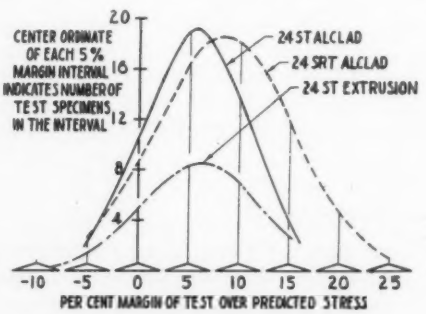

FIG. 7. Margin frequency curves.

TABLE 3 (*Continued*)
24S-RT Alclad Stiffeners, 24S-T Alclad Sheet

1	2	3	4	5	6	7	8
Stiffener*	Stiffener Gauge, t_{st}	Sheet† Gauge, t_{sh}	F_{cc}', Lbs. per Sq.in., Test Corrected	F_{ccl}, Lbs. per Sq.in.	K	Predicted $F_{cc} = KF_{ccl}$, Lbs. per Sq.in.	Margin, $\left(\frac{F_{cc}'}{F_{cc}} - 1\right)100$
X-785-B	0.025		21,600	17,600	1.08	19,000	13.7
	0.040		30,100	25,800	1.08	27,800	8.3
	0.064		41,200	36,700	1.08	39,600	4.0
X-785-C	0.025		22,000	19,500	0.92	17,900	22.9
	0.040		29,200	29,200	0.92	26,800	9.0
	0.064		43,500	42,200	0.92	38,800	12.1
X-785-D	0.025		24,300	22,500	1.08	24,300	0
	0.040		36,200	32,100	1.08	34,600	4.6
	0.064		52,700	43,700	1.08	47,200	11.7
LS 156	0.025	0.025	25,100	22,600	1.08	24,400	2.9
	0.032	0.025	28,200	25,000	1.08	27,000	4.4
	0.032	0.032	27,000	24,000	1.08	25,900	4.2
	0.040	0.025	35,500	28,200	1.08	30,400	16.8
	0.040	0.032	34,400	27,000	1.08	29,200	17.8
	0.040	0.040	33,000	25,800	1.08	27,800	18.7
LS 157	0.050	0.040	34,500	29,500	1.08	31,800	8.5
	0.051	0.051	30,000	27,800	1.08	30,000	0
	0.064	0.032	37,800	33,600	1.08	36,300	4.1
	0.064	0.040	41,500	32,200	1.08	34,800	19.3
	0.064	0.051	39,000	30,600	1.08	33,000	18.2
LS 152	0.040		39,500	40,900	0.92	37,600	5.1
	0.040	0.040	34,300	35,600	0.92	32,800	4.6
	0.040	0.051	32,900	34,400	0.92	31,600	4.1
LS 153	0.051		44,100	43,100	0.92	39,600	11.4
	0.051	0.040	39,200	39,400	0.92	36,200	8.3
	0.051	0.051	37,500	37,500	0.92	34,500	8.7
	0.051	0.064	37,000	36,200	0.92	33,300	11.1
LS 154	0.064	0.051	43,700	40,300	0.92	37,100	17.8
	0.064	0.064	42,600	39,400	0.92	36,200	17.7
LS 174	0.032	0.025	27,400	27,000	0.92	24,800	10.5
	0.040	0.040	24,100	27,100	0.92	24,900	− 3.2

* Sketches shown drawn to scale in Table 1. † No sheet gauge given indicates stiffener tested alone.

curves constructed by indicating on the ordinate the number of specimens having margins lying within each 5 per cent increment on the abscissa and then faired by statistical methods to give the normal form. Note that there are relatively few extruded stiffener combinations. Information from Tables 2, 3, 4, and Fig. 7 is summarized in Table 5. The positive margins of 6 to 9 per cent at the peak of the frequency curve indicate that if the method of this paper is used for a number of stiffeners and panels throughout an airplane, the average over strength of the stiffeners and panels will be only 6 to 9 per cent.

Test results show that as much as 6.5 per cent difference may occur between the crippling stress of identical specimens. On the whole the results appear good; however, it is felt the scatter would have been less had pin-ended tests been made instead of flat-ended ones and had all stiffeners and panels had exactly the same L/ρ for the nominal $L/\rho = 20$. Furthermore, it should be pointed out that the stiffeners tested alone had no lateral restraint and, consequently, failed about the axis of least radius of gyration.

Drawing the straight line column curve through F_{cc} and $L/\rho = 20$ is rather conservative in some cases. It is for this reason that making the construction through F_{cc} and $L/\rho = 40$ is suggested for the extrusion stiffened panel curves (note panel); in fact, such a construction approximates the parabolic form which the extrusion stiffened panel test points seem to follow.

Range of Application as Applied to Stiffener Design

The solid portions of the curves of Figs. 2 and 3 represent the range of tests for those curves; the dotted portions are extrapolations based on theory.

A summary of the b/t and R/t ranges is given in Table 6.

The writer feels that the extrapolated portions of the curves may be used providing the stiffeners so designed have good proportions. The following miscellaneous remarks on stiffener design should clarify the preceding statement:

(1) Avoid relatively long outstanding legs. The point marked(‡) in Table 2 is a good example where this rule was not followed, and the stiffener had poor

TABLE 4

24S-T Extruded Shapes, 24S-T Alclad Sheet

1 Stiffener*	2 Stiffener Gauge, t_{st}	3 Sheet† Gauge, t_{sh}	4 F_{cc}', Lbs. per Sq.in., Test Corrected	5 F_{ccl}, Lbs. per Sq.in.	6 K	7 Predicted $F_{cc} = KF_{ccl}$, Lbs. per Sq.in.	8 Margin, $\left(\frac{F_{cc}'}{F_{cc}} - 1\right)100$
Bulb Angles							
LS 222			30,400	27,900	1.08	30,200	0.7
Double 222		0.020	31,000	25,300	1.08	27,300	13.6
222		0.020	33,000	26,200	1.08	28,300	16.6
222		0.025	28,700	24,500	1.08	26,400	8.7
Double 222		0.025	30,500	25,600	1.08	27,600	10.5
222		0.032	26,000	23,400	1.08	25,300	2.8
222		0.040	22,400	22,600	1.08	24,400	− 8.2
220			31,800	29,500	1.08	31,800	0
220		0.020	31,700	27,700	1.08	29,900	6.0
Double 220		0.020	35,000	28,800	1.08	31,100	12.5
220		0.040	29,100	24,000	1.08	25,900	12.4
223			31,600	29,500	1.08	31,800	− 0.6
224			38,000	30,100	1.08	32,500	16.9
Bulb Tees							
LS 247			29,200	25,500	1.08	27,500	6.2
248			28,000	25,300	1.08	27,400	2.2
249			32,200	28,400	1.08	30,600	5.2
234			40,100	34,000	1.08	36,800	9.0
Angles 209			30,700	30,600	1.00	30,600	0.3
200			34,400	33,600	1.00	33,600	2.4
219			40,100	36,600	1.00	36,600	9.6
208			32,400	31,900	1.00	31,900	1.6
210			32,800	31,000	1.00	31,000	5.8
Channel 264			36,000	32,900	1.00	32,900	9.4
Tees 236			31,000	28,600	1.00	28,600	8.4
232			39,000	35,600	1.00	35,600	9.6

* Sketches shown drawn to scale in Table 1. † No sheet gauge given indicates stiffener tested alone.

TABLE 5

Type Stiffener	Number* Combinations	Range* of Test Margins, %	Margin at Which Peak of Normal Frequency Curve Occurs, %	Specimens from −2.5 to +17.5% Margin, Fig. 7 Number	Specimens from −2.5 to +17.5% Margin, Fig. 7 % Total	Specimens from −2.5 to +12.5% Margin, Fig. 7 Number	Specimens from −2.5 to +12.5% Margin, Fig. 7 % Total	Probable Variation of Single Prediction from Peak, ±%
24S-T Alclad Sheet	50	−4 to +16	5.7	47	94	43	86	3.5
24S-RT Alclad Sheet	64	−6 to +23	8.5	55	86	43	68	4.6
24S-T Extrusion	25	−8 to +17	6.2	23	92	20	81	4.0

* Two exceptions of Table 2 excluded.

TABLE 6

Range of Stiffener Tests

Type Stiffener	b/t No Edge Free	b/t One Edge Free	R/t No Edge Free	R/t One Edge Free
24S-T Alclad Sheet	0.9–45.2	3.1–28.9	3.2–10.5	3.6–8.4
24S-RT Alclad Sheet	8.8–42.9	0.6–27.7	3.0–10.6	4.8–8.3
24S-T Extrusion	22.0	6.0–19.0		

proportions. A little judgment is the best guide here (as elsewhere). This statement is particularly true in using the curves of Figs. 2 and 3 with extruded stiffeners of unusual shape and size, *since all the extrusions tested had legs of equal thickness* with a limited range of b/t.

(2) Use vertical-legged stiffeners when possible. Table 1 shows them to be more efficient, as would be expected.

(3) Make stiffener thicker than sheet by one gauge at least when possible. The tests indicate that for pure compression load a panel of heavy stiffeners and fabric covering would likely be the most efficient structure on the basis of strength-weight ratio. The point marked (**) in Table 2 shows the rule just stated should be rigidly followed in the instance of slant-legged stiffeners where the angle is considerably off the vertical as is that of the LS 174 stiffener. Some of the J-stiffener tests indicate that stiffener *thinner* than sheet by one gauge at most may be used for vertical-legged stiffeners, although not as efficiently as if the sheet were thinner

than the stiffener. As stated previously, the tendency of the sheet to form waves across the stiffener increases with the thickness of the sheet.

(4) Use flanges on the outstanding legs of stiffeners for making the one-edge-free element perpendicular to the sheet. This step increases the crippling stress, but may be undesirable from the production point of view.

Conclusion

If in the future the curves given herein are extended and the scatter reduced by making pin-ended tests, it may be possible to eliminate many panel tests, which should be the case for numerous applications of the present method. Even so, it is hoped the article as it stands will be of real assistance to structures engineers in predicting panel crippling stresses.

References

[1] ANC-5, *Strength of Aircraft Elements*, October, 1940, Edition.

[2] Niles, A. S., and Newell, J. S., *Airplane Structures*, 2nd Edition, Vol. I, p. 287; John Wiley & Sons, Inc., New York, 1938.

[3] Fischel, J. Robert, *The Compressive Strength of Thin Aluminum Alloy Sheet in the Plastic Region*, Journal of the Aeronautical Sciences, Vol. 8, No. 10, p. 373, August, 1941.

[4] Templin, R. L., Sturm, R. G., Hartmann, E. C., and Holt, M., *Column Strength of Various Aluminum Alloys*, Aluminum Company of America Technical Paper, No. 1, 1938.

[5] Reddick, H. W., and Miller, F. H., *Advanced Mathematics for Engineers*, p. 337; John Wiley & Sons, Inc., New York, 1938.

[6] Arkin, H., and Colton, R. R., *An Outline of Statistical Methods*, 4th Edition, p. 111; Barnes & Noble, New York, 1939.

Rational Analysis of Tension-Field Beams

H. W. SIBERT*
University of Cincinnati

SUMMARY

The analysis in this paper is not based upon Wagner's fundamental assumption that the force in each flange of a tension-field beam is in the direction of the flange. The wing is considered as a whole, and the stresses in the tension-field shear web are determined by a method similar to that for finding the longitudinal shear stresses in a beam with a shear-resistant web. Approximate formulas are then developed which can be applied to beams of either constant or variable cross section.

INTRODUCTION

THE COMMONLY ACCEPTED THEORY of tension-field beams was first given by Wagner[1, 2, 3] and was later summarized by Kuhn.[4] Wagner's theory is based upon the assumption that the force in each flange of a tension-field beam is in the direction of the flange. It will be shown later that Wagner's analysis gives the correct solution for a particular type of beam of constant cross section. For all other beams his analysis will give erroneous results.

Wagner's fundamental assumption is the result of an attempt to simplify the problem of the bending of a metal wing by assigning different functions to the different parts of the wing—namely, the bending moment is to be resisted by the flange material and the vertical shear by the shear web in conjunction with the vertical components of the forces in the flanges. In this paper the wing is considered as a whole and the stresses in the tension-field shear web are determined by a method similar to that for finding the longitudinal shear stresses in a beam with a shear-resistant web.

This paper will consider only beams with a single tension-field shear web. The more complicated problem of a beam with more than one shear-carrying member will be treated in a subsequent paper.

CANTILEVER BEAM WITH A SINGLE TENSION-FIELD SHEAR WEB

Consider a cantilever beam with a single tension-field shear web. Let the x (horizontal) axis pass through the center of gravity of the entire flange portion of each cross section, and let all the external loads be perpendicular to the x axis. Let A_F be the total area of the flange portion of a cross section at distance x from the free end of the beam. Fig. 1 shows the bending stresses f_b acting on A_F when the beam is bent upward by its external loads. The horizontal tensile stresses X in the web (due to the diagonal tensile stresses in the direction of the wrinkles) have been replaced by their moment M_W about the center of gravity of A_F and their resultant H_W acting through this center of gravity.

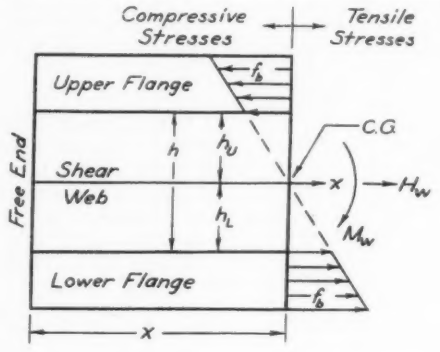

FIG. 1.

Let M and M_b be the moments about the center of gravity of A_F of the external loads and of the stresses f_b in A_F, respectively. M is positive when causing compression in the upper fiber, M_b is positive when f_b in the upper fiber is compressive, and M_W is positive when the moment of the horizontal tensile stresses X on the portion of the web above the center of gravity of A_F exceeds the moment of X on the portion of the web below this c.g. Because of these sign conventions

$$M_b - M_W = M \qquad M_b = M + M_W \tag{1}$$

because the two internal moments, M_b and M_W, must balance the external moment M.

In the following analysis all stresses and forces perpendicular to a cross section are positive when tensile. Let A_U be the area of the upper portion of A_F, and let R_U be the resultant of the bending stresses f_b on A_U. Since M_b is positive when f_b is compressive in the upper fiber while f_b and R_U are positive when tensile, it is evident from Eq. (1) that

$$f_b = -M_b y/I = -(M + M_W)y/I \tag{2}$$

$$R_U = \int_{AU} f_b dA = -(M + M_W)Q_U/I \tag{3}$$

where y is the distance of f_b from the center of gravity of A_F, I is the moment of inertia of A_F, and Q_U the moment of A_U about this center of gravity.

Since the resultant tensile force, H_W, on the shear web acts through the center of gravity of the flange area A_F, it must be balanced by a direct compressive stress, $-f_d$, distributed uniformly over A_F. Let P_U be the

Received March 16, 1942.

* Associate Professor of Mathematics and Aeronautics.

resultant force due to stress f_d on A_U. Since f_d, H_W and P_U are positive when tensile,

$$f_d = -H_W/A_F \qquad P_U = f_d A_U = -H_W A_U/A_F \quad (4)$$

Fig. 2 shows the horizontal forces and stresses (in their positive directions) acting on a portion of the beam bounded by two vertical planes at distances x and $x + dx$ from the unsupported end and by a third plane through the wrinkle (at angle α with the x axis) which passes through the top of the shear web at the left face of Fig. 2. As shown in Fig. 2, this wrinkle extends downward to the right because the beam was assumed to be bent upward by its external loads. X_U is the value of X at the intersection of the top of the shear web with the left face of Fig. 2.

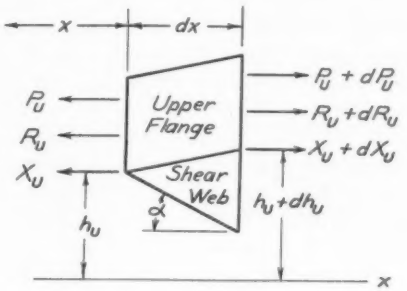

FIG. 2.

Let t be the thickness of the shear web. Since Wagner[1] has shown that there can be no stress along a cut parallel to the wrinkles of a tension-field web, the result of equating to zero the sum of the forces in Fig. 2 in the x direction is

$$X_U t(dx \tan \alpha + dh_U) + dR_U + dP_U = 0 \quad (5)$$

$$X_U t(\tan \alpha + h_U') = -d(R_U + P_U)/dx \quad (6)$$

where $h_U' = dh/dx$. Replacing R_U and P_U by their values given in Eqs. (3) and (4)

$$tX_U(\tan \alpha + h_U') = d\{[(M + M_W)Q_U/I] + H_W A_U/A_F\}/dx \quad (7)$$

For a beam of constant cross section, h_U, Q_U/I and A_U/A_F are all constant and Eq. (7) reduces to

$$tX_U \tan \alpha = [(S + M_W')Q_U/I] + H_W' A_U/A_F \quad (8)$$

where $S = dM/dx$ is the total shear force on the cross section, $M_W' = dM_W/dx$ and $H_W' = dH_W/dx$.

By virtue of the sign convention for M_W and the fact that X and H_W are positive when tensile,

$$H_W = \int_{-h_L}^{h_U} Xt\,dy \qquad M_W = \int_{-h_L}^{h_U} yXt\,dy \quad (9)$$

where y is the distance of X from the c.g. of A_F, and h_U and h_L are, respectively, the distances from the c.g. of A_F to the top and bottom of the shear web (Fig. 1). Letting $X' = dX/dx$,

$$H_W' = \int_{-h_L}^{h_U} X't\,dy \qquad M_W' = \int_{-h_L}^{h_U} yX't\,dy \quad (10)$$

Fig. 3 shows a tension-field shear web of a cantilever beam bent upward under the action of external loads. Consider a cross section at distance x from the free end of the beam. Since all stresses are constant along a wrinkle, the horizontal stress X at any point A on this cross section is the same as X_U at the top of the shear web (point B) on a second cross section. Thus, the determination of X_U at the top of the shear web at each cross section by means of Eq. (7) or (8) will define X at any point on a desired cross section, except when a wrinkle through that point fails to intersect the upper boundary of the shear web. However, this situation occurs only on cross sections near the free end where the web stresses are generally much smaller than at cross sections at greater distances from the free end.

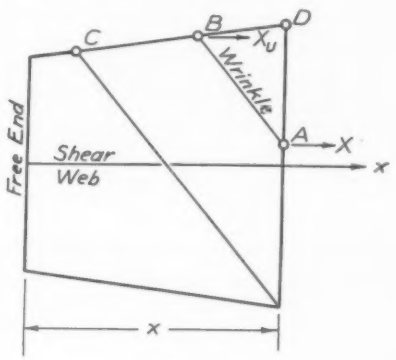

FIG. 3.

WAGNER BEAMS

In this article tension-field beams in which the centers of gravity of the upper and lower flanges fall, respectively, at the top and bottom of the shear web will be called Wagner beams (Wagner[1] makes this very assumption in his analysis of tension-field beams). If A_L is the area of the lower portion of A_F and if the moment of inertia of A_U and A_L about their own centers of gravity are neglected, the following relations hold for a Wagner beam

$$h_U A_U = h_L A_L \qquad I = h_U^2 A_U + h_L^2 A_L \qquad Q_U = h_U A_U \quad (11)$$

because h_U and h_L are now the distances of the centers of gravity of A_U and A_L, respectively, from the center of gravity of A_F. By virtue of the relation $h_U A_U = h_L A_L$ it can be shown that

$$I = (h_U + h_L)h_U A_U = hQ_U \qquad A_U/A_F = h_L/h \quad (12)$$

The substitution in Eq. (7) of $1/h$ for Q_U/I and h_L/h for A_U/A_F gives an equation from which X_U for a tapered Wagner beam can be found for many loading conditions. For the sake of simplicity, the actual deter-

mination of X_U for various loading conditions will be limited to Wagner beams of constant cross section.

Wagner Beam of Constant Cross Section

From Eqs. (8), (10) and (12) the value of X_U for a Wagner beam of constant cross section is

$$htX_U \tan \alpha = S + \int_{-h_L}^{h_U} tX'(y + h_L)dy \qquad (13)$$

Kuhn[4] has found that α is approximately 45 deg. for tension-field beams similar to those found in airplane wings. For the sake of simplicity, this value of α will be used in the analysis which follows.

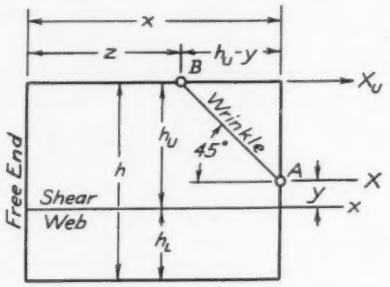

Fig. 4.

Fig. 4 shows a portion of a Wagner beam of constant cross section. The stress X at point A on a cross section at distance x from the free end is equal to X_U at point B, whose distance z from the free end is a function of y. In fact (Fig. 4),

$$y = h_U - x + z \qquad dy = dz \qquad (14)$$

In Eq. (13) let $\alpha = 45$ deg. and change the variable in the integral from y to z by means of Eq. (14). The final result is

$$htX_U = S + \int_{x-h}^{x} tX_U'(h - x + z)dz \qquad (15)$$

where X_U' is the value of dX_U/dx with each x replaced by a z. Since both x and z are horizontal distances from the free end of the beam, this definition of X_U makes $X_U'dz = dX_U$. After $X_U'dz$ in Eq. (15) is replaced by dX_U, an integration by parts reduces this equation to

$$\int_{x-h}^{z} tX_U\,dz = S \qquad (16)$$

A change of variable in Eq. (16) from z to y by means of Eq. (14) gives

$$\int_{-h_L}^{h_U} tX\,dy = S \qquad (17)$$

Wagner[1] shows that $X = \tau$ when $\alpha = 45$ deg., τ being the equivalent vertical shear stress in the web. Hence, Eq. (17) proves that the entire shear force S on a cross section of a Wagner beam of constant cross section is carried by the shear web. Moreover, the same result will be reached when α is not 45 deg.

Wagner's assumption that the shear force in each flange is parallel to the flange leads to the same conclusion when the beam is of constant cross section. Hence, for Wagner beams of constant cross section, Wagner's assumption and the analysis developed in this article give identical results. However, the results will not be the same for beams other than Wagner beams of constant cross section.

Approximate Formula for Beams of Constant Cross Section

When a beam of constant cross section is not of the Wagner type, X must be found from Eq. (8). Since H_W' and M_W' are functions of X' (Eq. (10)), the determination of X from Eq. (8) requires the solution of an integral equation. In airplane wings SQ_U/I generally contributes much more to X than the two remaining terms combined. This fortunate situation permits a solution of Eq. (8) by successive approximations. The resulting formula is comparatively simple if only two approximations are used. This formula will be in still simpler form if $\alpha = 45$ deg., which is the approximate value of α for tension-field beams in airplane wings.[4] The first approximation is obtained by letting $X_U = X_{UO}$ in Eq. (8) and putting $X' = 0$ in H_W' and M_W' (Eq. (10)). Then, with $\alpha = 45$ deg., Eq. (8) becomes

$$tX_{UO} = SQ_U/I \qquad (18)$$

From Eq. (18) $tX_{UO}' = wQ_U/I$, where $w = dS/dx$ is the external load per unit length of beam (positive when upward).

The second approximation results from putting $tX' = wQ_U/I$ in P_W' and M_W' (Eq. (10)). With $\alpha = 45$ deg., this changes Eq. (8) into

$$tX_U = (S + \phi)Q_U/I \qquad (19)$$

$$\phi = (Q_U/I)\int_{-h_L}^{h_U} yw\,dy + (A_U/A_F)\int_{-h_L}^{h_U} wdy \qquad (20)$$

Eqs. (19) and (20) were obtained by replacing tX' in Eq. (10) by wQ_U/I. Actually, $tX_{UO}' = wQ_U/I$. However, the X' at any point A on a cross section is the same as the X_U' at point B on the upper edge of the shear web when AB is a wrinkle through point A (Figs. 3 and 4). Hence, the w to use at point A is the load per unit length of span at point B (Figs. 3 and 4). Thus, w in Eq. (20) varies from the load per unit length of span at point C to the load per unit length of span at point D (Fig. 3). It will be convenient to call these two loads per unit length of span w_L and w_U, respectively. Since the spanwise distance between C and D (Fig. 3) is approximately equal to the height of the beam and since the ratio of beam height to beam length is small in airplane wings, there should be little error in assuming a straight line variation of w between w_L and w_U.

If this is done, Eq. (20) reduces to

$$\phi = [(w_1/2) - (w_m h_L/h)](h^2 Q_U/I) + (w_m h A_U/A_F) \quad (21)$$

$$w_m = (w_U + w_L)/2 \qquad w_1 = (2w_U + w_L)/3 \quad (22)$$

Thus, w_m and w_1 are, respectively, the loads per unit length of span midway between C and D and one-third of the way from D to C (Fig. 3).

Approximate Formula for Beams of Variable Cross Section

The ratio A_U/A_F in Eq. (7) should be practically constant for most airplane wings. If A_U/A_F is taken constant and $\alpha = 45$ deg., the application of the formula for the derivative of the product of two variables to Eq. (7) gives

$$tX_U(1 + h_U') = [(S + M_W')Q_U/I] + [(M + M_W)d(Q_U/I)/dx] + H_W' A_U/A_F \quad (23)$$

Little error should result from neglecting M_W in Eq. (23) because M_W is always small numerically compared with M if the cross section in question is not close to the free end of the beam. With M_W neglected, Eq. (23) becomes

$$tX_U(1 + h_U') = [(S + M_W')Q_U/I] + [(H_W' A_U/A_F) + Md(Q_U/I)/dx] \quad (24)$$

The dimensions of Q_U and I are cu.in. and in.^{4}, respectively. Since the height h of an airplane wing increases as the distance x from the free end increases, Q_U/I decreases as x increases and $d(Q_U/I)/dx$ is negative. Moreover, since M is positive when the free end of the beam is bent upward under the action of its external loads, $Md(Q_U/I)/dx$ will be negative for such a beam. Since h increases as x, h_U also increases with x and h_U' is positive. It would be on the side of safety, then, to neglect both $Md(Q_U/I)/dx$ and h_U' in Eq. (24). If this is done, Eq. (24) becomes

$$tX_U = [(S + M_W')Q_U/I] + H_W' A_U/A_F \quad (25)$$

which is identical with Eq. (8). Since Eq. (19) is a close approximation of Eq. (8), it is also a close approximation of Eq. (25). The neglected terms, h_U' and $Md(Q_U/I)/dx$, can now be introduced into Eq. (19) in the same places as they were in Eq. (24). Eq. (19) then becomes

$$tX_U(1 + h_U') = [(S + \phi)Q_U/I] + Md(Q_U/I)/dx \quad (26)$$

where ϕ is defined by Eq. (21).

A more accurate approximation of Eq. (24) could have been found by letting $X' = 0$ in M_W' and H_W' (Eq. (10)) to obtain the following first approximation of X_U:

$$tX_{UO}(1 + h_U') = (SQ_U/I) + Md(Q_U/I)/dx \quad (27)$$

A second approximation could then be found by putting $X' = X_{UO}'$ in M_W' and H_W', which would lead to a more accurate equation than Eq. (26). However, Eq. (26) is simpler and also conservative, because the value $tX_{UO} = SQ_U/I$ (Eq. (18)) used in the derivation of Eqs. (19) and (26) is larger than the value of tX_{UO} obtainable from Eq. (27).

For Wagner beams $I/Q_U = h$ (Eq. (12)). This relation does not hold in general, but it is probably true that for most airplane wings I/Q_U is proportional to h, or $I/Q_U = kh$, where k is a constant of proportionality. By virtue of this relation,

$$d(Q_U/I)/dx = -h'/kh^2 = -(h'/h)Q_U/I \quad (28)$$

where $h' = dh/dx$. The substitution of this value of $d(Q_U/I)/dx$ in Eq. (26) gives

$$tX_U(1 + h_U') = (S + \phi - Mh'/h)Q_U/I \quad (29)$$

where ϕ is defined by Eq. (21). Since M and h' are positive in airplane wings, Mh'/h is positive. Hence, the stress X_U at a given cross section of a tapered wing is always less than in a beam of the same height whose cross section is constant.

For a Wagner beam $I/Q_U = h$ and $A_U/A_F = h_L/h$ (Eq. (12)). The substitution of these values in Eqs. (21) and (29) reduces Eq. (29) to

$$tX_U(1 + h_U') = (S/h) + (w_1/2) - (Mh'/h^2) \quad (30)$$

where w_1 is defined by Eq. (22). For a Wagner beam of constant cross section $h_U' = h' = 0$ and Eq. (30) becomes

$$tX_U = (S/h) + (w_1/2) \quad (31)$$

Accuracy of Approximate Formulas

Before the accuracy of the approximate formulas heretofore developed can be checked, the corresponding exact solutions must be known. For the sake of simplicity, only the approximate formula for a Wagner beam of constant cross section (Eq. (31)) will be checked. The following loading conditions will be considered: (a) concentrated load P at end of beam—$S = P$; (b) uniform load—$w = k$, $S = kx$; (c) uniformly varying load—$w = kx$, $S = kx^2/2$; (d) parabolic load—$w = kx^2$, $S = kx^3/3$; (e) cubical load—$w = kx^3$, $S = kx^4/4$.

The following exact values of X_U satisfy both Eq. (15) and Eq. (16): (a) concentrated load—$tX_U = P/h$; (b) uniform load—$tX_U = k[(x/h) + (1/2)]$; (c) uniformly varying—$tX_U = k[(x^2/2h) + (x/2) + (h/12)]$; (d) parabolic load—$tX_U = k[(x^3/3h) + (x^2/2) + (hx/6)]$; (e) cubical load—$tX_U = k[(x^4/4h) + (x^3/2) + (hx^2/4) - (h^3/120)]$.

Since w_1 in Eq. (31) is the load per unit length of span at $x - h/3$ (Eq. (22)), the following approximate values of X_U are obtained from Eq. (31): (a) concentrated load—$tX_U = P/h$; (b) uniform load—$tX_U = (kx/h) + (k/2)$; (c) uniformly varying—$tX_U = (kx^2/2h) + [k(x - h/3)/2]$; (d) parabolic load—

$tX_U = (kx^3/3h) + [k(x - h/3)^2/2]$; (e) cubical load—$tX_U = (kx^4/4h) + [k(x - h/3)^3/2]$.

A comparison of the exact and approximate values of X_U shows that Eq. (31) gives no error for a concentrated or uniform load, while the error in the other three cases are: (c) uniformly varying—$kh/4$; (d) parabolic load—$k[(hx/2) - (h^2/18)]$; (e) cubical load—$k[(3hx^2/4) - (h^2x/6) + (11h^3/1080)]$.

A comparison of the first term of each error with the first term of the corresponding exact solution shows that the relative error cannot exceed the following values: (c) $0.5(h/x)^2$; (d) $1.5(h/x)^2$; (e) $3(h/x)^2$. Hence, toward the root of an airplane wing where h/x is small and X_U has its largest values, the relative error in using Eq. (31) for these three loadings is extremely small.

The error from using the approximate formulas for beams other than Wagner beams could be obtained by finding exact solutions from Eqs. (7) and (8). However, an estimate of the accuracy of these approximate formulas without first finding the exact solution can be made in the following manner. The term ϕ in Eqs. (19) and (29) is the additional term that is added to the first approximation to obtain the final approximate solution. The error involved in neglecting all successive approximations after the second ought not to exceed ϕ. Hence, if ϕ turns out to be small compared with the first approximation, the error itself should be small compared with the first approximation.

Total Stress in Flanges

With X known at each point on a cross section, H_W and M_W for the cross section can be determined from Eq. (9). Since the height of an airplane wing is always small compared with its length, not much error should result in H_W or M_W if X is assumed to vary as a straight line from X_L at the bottom to X_U at the top of the shear web. With this simplification, Eq. (9) becomes

$$H_W = X_m th \qquad M_W = [(X_1/2) - (X_m h_L/h)]th^2 \quad (32)$$

$$X_m = (X_U + X_L)/2 \qquad X_1 = (2X_U + X_L)/3 \quad (33)$$

Note that X_m is the stress at the midpoint of the shear web while X_1 is the stress one-third down from the top of the web.

After H_W and M_W have been found from Eq. (32), the total stress f_t at any point on the flange is (Eqs. (2) and (4))

$$f_t = f_b + f_d = -[(M + M_W)y/I] - H_W/A_F \quad (34)$$

There is no need to make any correction for the vertical component of the forces in the flanges as is done in Wagner's analysis, because all stresses have been included in Eq. (34).

References

[1] Wagner, Herbert, *Flat Sheet Metal Girder with Very Thin Metal Web*, Part I, N.A.C.A. T.M. No. 604, February, 1931.

[2] Wagner, Herbert, *Flat Sheet Metal Girder with Very Thin Metal Web*, Part II, N.A.C.A. T.M. No. 605, February, 1931.

[3] Wagner, Herbert, *Flat Sheet Metal Girder with Very Thin Metal Web*, Part III, N.A.C.A. T.M. No. 606, February, 1931.

[4] Kuhn, Paul, *A Summary of Design Formulas for Beams Having Thin Webs in Diagonal Tension*, N.A.C.A. T.N. No. 469, August, 1933.